Article

Cell

Cellular Cholesterol Directly Activates Smoothened in Hedgehog Signaling

Graphical Abstract

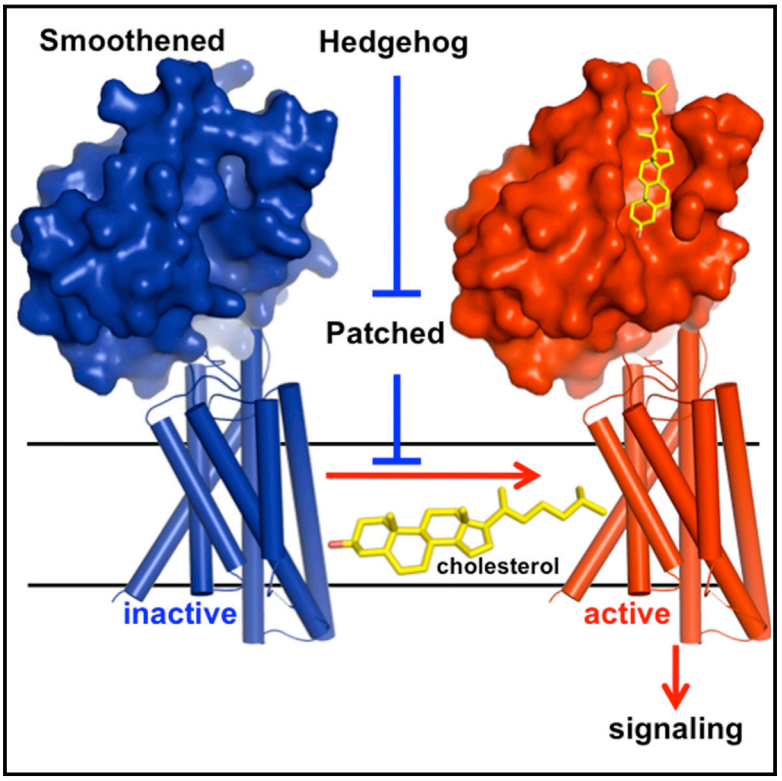

Authors

Pengxiang Huang, Daniel Nedelcu, Miyako Watanabe, Cindy Jao, Youngchang Kim, Jing Liu, Adrian Salic

Correspondence

asalic@hms.harvard.edu

In Brief

Although Smoothened can bind to several different sterols, cholesterol serves as its endogenous activator, driving a conformational change in the protein that enables Hedgehog signaling.

Highlights

- Sterol-induced conformational change in Smoothened triggers Hedgehog signaling
- Cholesterol is the endogenous activator of Smoothened
- Stimulation of Hedgehog pathway activates Smoothened through cholesterol

Data Resources

5KZZ
5KZV
5KZY

Huang et al., 2016, Cell *166*, 1176–1187
August 25, 2016
http://dx.doi.org/10.1016/j.cell.2016.08.003

CellPress

Cell

Article

Cellular Cholesterol Directly Activates Smoothened in Hedgehog Signaling

Pengxiang Huang,[1] Daniel Nedelcu,[1] Miyako Watanabe,[1] Cindy Jao,[1] Youngchang Kim,[2] Jing Liu,[1] and Adrian Salic[1,3,*]
[1]Department of Cell Biology, Harvard Medical School, 240 Longwood Avenue, Boston, MA 02115, USA
[2]Structural Biology Center, Biosciences Division, Argonne National Laboratory, Argonne, Illinois 60439, USA
[3]Lead Contact
*Correspondence: asalic@hms.harvard.edu
http://dx.doi.org/10.1016/j.cell.2016.08.003

SUMMARY

In vertebrates, sterols are necessary for Hedgehog signaling, a pathway critical in embryogenesis and cancer. Sterols activate the membrane protein Smoothened by binding its extracellular, cysteine-rich domain (CRD). Major unanswered questions concern the nature of the endogenous, activating sterol and the mechanism by which it regulates Smoothened. We report crystal structures of CRD complexed with sterols and alone, revealing that sterols induce a dramatic conformational change of the binding site, which is sufficient for Smoothened activation and is unique among CRD-containing receptors. We demonstrate that Hedgehog signaling requires sterol binding to Smoothened and define key residues for sterol recognition and activity. We also show that cholesterol itself binds and activates Smoothened. Furthermore, the effect of oxysterols is abolished in Smoothened mutants that retain activation by cholesterol and Hedgehog. We propose that the endogenous Smoothened activator is cholesterol, not oxysterols, and that vertebrate Hedgehog signaling controls Smoothened by regulating its access to cholesterol.

INTRODUCTION

The Hedgehog (Hh) cell-cell signaling pathway controls key events in the development of most animals. Insufficient Hh activity during embryogenesis causes birth defects such as holoprosencephaly and brachydactyly, while hyperactive Hh signaling after birth is implicated in many cancers (Ingham and McMahon, 2001; Lum and Beachy, 2004), including basal cell carcinoma and medulloblastoma.

The oncoprotein Smoothened (Smo) (Alcedo et al., 1996; van den Heuvel and Ingham, 1996), a member of the Frizzled (Fz) family of seven-transmembrane domain (7TM) proteins, is critical for relaying Hh signals across the plasma membrane. In unstimulated cells, Smo is inhibited by the tumor suppressor membrane protein Patched (Ptch) (Nakano et al., 1989), thus ensuring that the Hh pathway is repressed. During Hh stimulation, the secreted Hh ligand binds and inhibits Ptch, leading to activation of Smo, which in turn, triggers the downstream signal transduction events of the Hh pathway, ultimately causing activation of target gene transcription.

A central unresolved question in Hh signaling is how Smo activity is controlled. Like other 7TM receptors, Smo functions as a conformational switch, equilibrating between inactive and active conformations. It has long been hypothesized this equilibrium is controlled by an unknown endogenous small molecule, which in turn, is regulated by Ptch (Taipale et al., 2002). Supporting this hypothesis, Ptch belongs to the resistance-nodulation-division (RND) family of small molecule pumps (Tseng et al., 1999), and residues required for activity in bacterial RND homologs (Murakami et al., 2006) are critical for Ptch function in suppressing Hh signaling (Taipale et al., 2002).

Recently, sterols have emerged as candidate endogenous activators of vertebrate Smo. Sterols are required for vertebrate Hh signaling, which is inhibited by sterol depletion or by genetic defects in cholesterol biosynthesis (Cooper et al., 2003). Furthermore, some oxysterols, compounds belonging to a poorly understood class of metabolites generated by cholesterol oxidation, activate Smo (Corcoran and Scott, 2006; Dwyer et al., 2007; Nachtergaele et al., 2012) by binding to a site located in its extracellular, cysteine-rich domain (CRD) (Myers et al., 2013; Nachtergaele et al., 2013; Nedelcu et al., 2013). Interestingly, vertebrate Smo harbors an additional small-molecule-binding site in its 7TM (Chen et al., 2002a; Wang et al., 2013), which binds synthetic agonists (such as SAG [Chen et al., 2002b; Frank-Kamenetsky et al., 2002] and purmorphamine [Sinha and Chen, 2006]) and antagonists (such as cyclopamine [Chen et al., 2002a] and SANT1 [Frank-Kamenetsky et al., 2002]); however, no endogenous small molecule is known to bind the 7TM site, whose physiological significance in Hh signaling thus remains unclear.

Naturally occurring oxysterols that activate Smo are 20(S)-hydroxycholesterol (20(S)-OHC, the most potent Hh-stimulating oxysterol) (Kim et al., 2007; Nachtergaele et al., 2012), 25-hydroxycholesterol (25-OHC) (Dwyer et al., 2007), 7-keto-25-hydroxycholesterol (7-keto-25-OHC) and 7-keto-27-hydroxycholesterol (7-keto-27-OHC) (Myers et al., 2013). It is unclear if any of these oxysterols are physiological activators of Smo, given their significantly lower endogenous levels than the EC_{50} for Hh pathway activation (Myers et al., 2013). Additionally, oxysterols such as 20(S)-OHC do not synergize with Hh ligand (Kim et al., 2007; Nachtergaele et al., 2012), as would be expected if they were involved in Smo regulation by Ptch. Together, these results

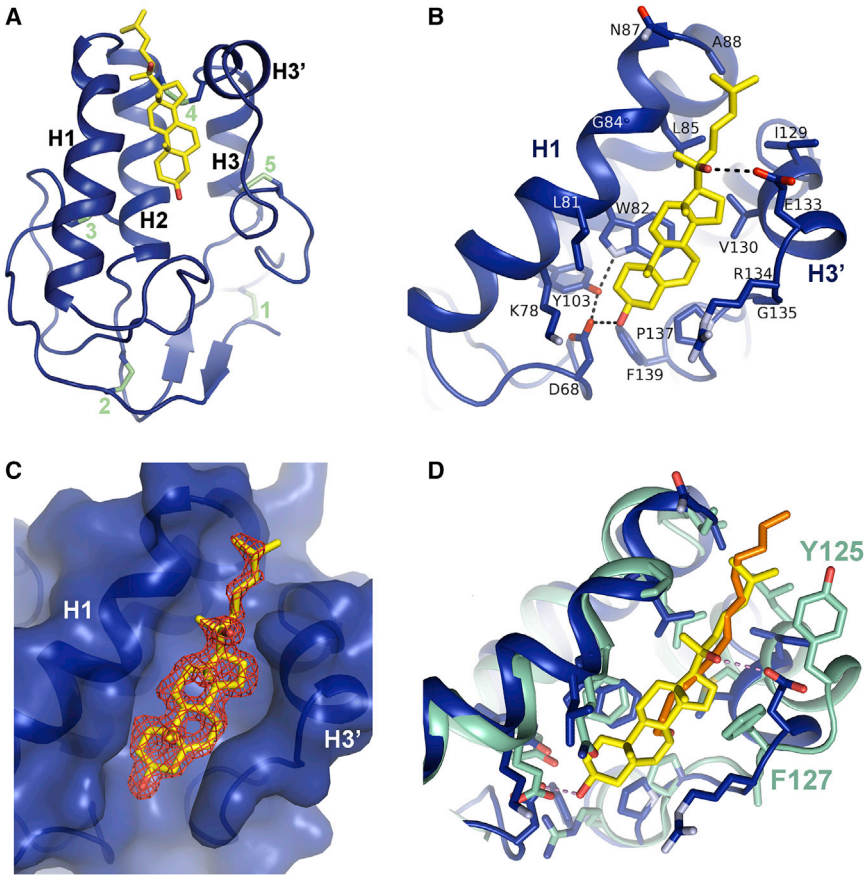

Figure 1. Structure of a SmoCRD-Oxysterol Complex

(A) Ribbon model showing overall structure of XSmoCRD (navy) in complex with 20(S)-OHC (yellow). Disulfide bonds (green) and the four helices are numbered.

(B) Contacts mediating 20(S)-OHC recognition. Hydrogen bonds involving the two hydroxyls of oxysterol (3β-OH bonded to D68 and 20-OH bonded to E133) are shown as dashed lines. See also Figure S2D and S2E for all Smo-sterol contacts.

(C) Shape complementarity of Smo sterol-binding site to 20(S)-OHC. Electron density of 20(S)-OHC (yellow oxysterol surrounded by red mesh, F_o-F_c omit map contoured at 3σ) is shown with the molecular surface of the sterol-binding site (blue). See also Figure S2F and S2H for binding site volume.

(D) Comparison between recognition of 20(S)-OHC by XSmoCRD and recognition of *Xenopus* Wnt8 palmitoyl moiety by mouse Fz8CRD (PDB ID 4F0A). Close-up view of sterol-binding site of XSmoCRD (navy), superimposed on palmitate-binding site of mFz8CRD (cyan). 20(S)-OHC (yellow) and palmitate (orange) occupy topologically equivalent sites. Two bulky residues in Helix 3 of mFz8, Y125 and F127, cause the palmitate-binding groove to be significantly narrower than the sterol-binding groove in XSmo. Additionally, the two charged residues responsible for polar recognition of oxysterols by XSmo, D68 and E133, are absent in mFz8. See also Figure S2F–S2I for comparison of ligand-binding site volume between XSmoCRD and mFz8CRD.

suggest that, perhaps, another sterol functions as endogenous ligand for Smo.

Three key unanswered questions are how Smo recognizes sterols, how sterols activate Smo, and most importantly, which endogenous sterol is involved in Smo activation during Hh signaling. Here, we use X-ray crystallography and functional approaches to elucidate these questions. We begin by solving the structure of SmoCRD bound to 20(S)-OHC, which we use to precisely define how Smo recognizes sterols. Smo mutants designed on basis of the structure are then used to demonstrate that sterol binding is essential for Hh signaling. We next solve the structure of unliganded SmoCRD, revealing that 20(S)-OHC induces a dramatic conformational change of the protein. We demonstrate that this conformational change is sufficient for Smo activation, revealing the mechanism by which sterol-bound CRD activates allosterically the 7TM domain, to trigger downstream signaling. Strikingly, we discover that cholesterol directly activates Smo and synergizes with Hh ligand. We also find that cholesterol hydroxylation on C-25, C-26, or C-27 is not absolutely required for Hh signaling, indicating that 25-OHC, 7-keto-25-OHC, or 7-keto-27-OHC are not essential for Smo activation. Finally, we use structure-guided mutagenesis to demonstrate that cholesterol, and not 20(S)-OHC, activates Smo in cells. Together, our results suggest that the endogenous activator of vertebrate Smo is cholesterol itself, providing the first instance in which cholesterol plays a second messenger role in a critical developmental signaling pathway. We propose that vertebrate Hh signaling through Ptch controls Smo by regulating its interaction with cholesterol.

RESULTS

Structure of SmoCRD Bound to Oxysterol

To understand Smo regulation by sterols, we focused on the interaction between SmoCRD and 20(S)-hydroxycholesterol (20(S)-OHC; Figure S1) (Kim et al., 2007; Nachtergaele et al., 2012). We purified the CRD of *Xenopus laevis* Smo (XSmoCRD), which recapitulates the sterol-binding properties of the larger XSmo ectodomain (Figure S2A–S2C). We then crystallized XSmoCRD in complex with 20(S)-OHC and solved its structure at 1.6-Å resolution (Table S1).

XSmoCRD adopts a characteristic Frizzled CRD fold, consisting of four α helices and a short two-strand β sheet, arranged in globular shape and stabilized by five conserved disulfide bonds (Figure 1A). The ligand occupies the proposed binding groove on the CRD surface (Bazan and de Sauvage, 2009), formed primarily by Helix 1 on one side, and Helix 3′ and the following loop region on the other (Figures 1B, S2D, and S2E). The A ring of the sterol molecule faces the bottom portion of the α-helical bundle (Figure 1A), while the isooctyl tail is positioned near the groove opening at the top: this orientation is opposite to the previous docking model (Nachtergaele et al., 2013) based on

the structure of zebrafish SmoCRD (zfSmoCRD). The smooth α face of 20(S)-OHC is completely buried, while the rough β face is largely exposed to solvent. The flat tetracyclic sterol core fits closely the shape of the binding site (Figures 1C and S2F). Our structure helps explain the mechanism of impaired oxysterol binding by previous point mutations in mSmoCRD (Table S2). A comparison with the structure of Frizzled-8 (Fz8) CRD bound to Wnt8 (Janda et al., 2012) shows that 20(S)-OHC and the palmitoyl moiety of Wnt8 occupy topologically equivalent sites in CRD (Figures 1D, S2F, and S2G). The sterol 3β-OH points in the same direction as the carboxyl head of palmitate, and the sterol isooctyl tail aligns with the hydrocarbon tail of palmitate. Though the CRD fold is conserved, the ligand-binding grooves in Smo and Fz8 have unique size, shape, and chemical properties, allowing them to discriminate their cognate lipid ligands (Figures S2F–S2I).

Oxysterol Recognition by Smo

In addition to sterol shape complementarity, XSmoCRD recognizes the two hydroxyls of 20(S)-OHC via hydrogen bonding (Figure 1B). The 3β-OH group, a salient feature of all sterols, forms a hydrogen bond with the conserved D68 residue, itself precisely positioned by a hydrogen bond network involving one of its carboxylate oxygen atoms, the hydroxyl group of Y103, and the indole nitrogen of W82. Mutating D99 in mouse Smo (mSmo), which corresponds to D68 in XSmo, abolishes sterol binding (Figure 2A), indicating that 3β-OH recognition via hydrogen bonding is crucial. Consistent with this result, D99 mutation selectively blocks activation of mSmo by the 20(S)-OHC analog, 20(S)-OHC-Pent (Nedelcu et al., 2013; Figure S1), while preserving robust activation by the synthetic agonist SAG (Chen et al., 2002b), which binds the 7TM of mSmo (Figure 2B). Crucially, mSmoD99A is unresponsive to Sonic Hedgehog (Shh) stimulation (Figure 2C), demonstrating that sterol binding to CRD is necessary for Smo activation in response to upstream signaling triggered by Shh binding to Patched1 (Ptch1).

The 20(S)-OH group is recognized via hydrogen bond with the conserved E133 residue (Figure 1B). Mutating the corresponding mSmo residue (mSmoE164L) greatly reduces 20(S)-OHC binding (Figure 2A) and significantly decreases activation by 20(S)-OHC-Pent (Figure 2D). In addition to 20(S)-OH binding by E133, the 20-methyl group contacts the backbone of residue G84 (Figures 1B and S2E). Positioning of E133 and G84 on opposite sides of the sterol binding groove suggests an explanation for the exquisite diastereoselectivity of Smo for 20(S)-OHC versus 20(R)-OHC (Nachtergaele et al., 2012; Nedelcu et al., 2013): binding of 20(R)-OHC would be energetically costly, due to loss of hydrogen bond with E133 and a clash between the 20-methyl group and E133 carboxylate. To test this hypothesis, we generated the G84S mutation, reasoning that the Ser side chain will hydrogen bond with the 20(R)-OH group, thereby stabilizing 20(R)-OHC binding. Indeed, purified XSmoG84S ectodomain displayed reversed diastereoselectivity compared to wild-type XSmo ectodomain, binding 20(R)-OHC preferentially over 20(S)-OHC (Figure S3). Strikingly, the corresponding mSmo mutant, mSmoG115S, was strongly activated by 20(R)-OHC (Figure 2E), in contrast to wild-type mSmo (Figure 2F). This result elucidates the mechanism of Smo diastereoselectivity and indicates that sterol configuration at C-20 is important for Smo binding but not for activation.

Sterol Binding Induces Conformational Change in SmoCRD

A comparison between our XSmoCRD-20(S)-OHC structure and that of unliganded zfSmoCRD (Nachtergaele et al., 2013) revealed no significant conformational change upon ligand binding (Figure S4A). However, the sterol-binding groove of zfSmoCRD is heavily involved in crystal packing (Figure S4B), suggesting that zfSmoCRD might have been inadvertently captured in a conformation similar to the sterol-bound state. We thus crystallized unliganded XSmoCRD in a form in which the sterol-binding site is not involved in crystal contacts and is completely solvent exposed and determined its structure at 1.3-Å resolution (Figures 3A and S4C; Table S1). A comparison between unliganded XSmoCRD and XSmoCRD-20(S)-OHC reveals that sterol binding induces a dramatic yet highly localized conformational change (Figure 3B; Movie S1), consisting of backbone rearrangement and side chain rotameric switches within the polypeptide segment anchored by Cys127 and Cys142, two residues involved in disulfide bonds 4 and 5. The most pronounced change involves a cluster of hydrophobic residues underneath the sterol rings (W136, P137, F139, and L140), with Cα displacements of up to 7.0 Å (Figure 3C). The end result of these movements is formation of a complete binding cavity that encloses the sterol. The ligand-induced conformational change we observed in Smo is unique among CRD-containing proteins; for example, mFz8CRD conformation does not change upon Wnt8 binding (Janda et al., 2012).

SmoCRD Conformational Change Is Sufficient for Smo Activation

The sterol-induced conformational change in SmoCRD suggests a mechanism for Smo activation by oxysterols. We hypothesized that CRD conformational change is relayed to the 7TM domain of Smo, which then switches to an active conformation that triggers downstream signaling. This model predicts that non-oxysterol compounds that bind SmoCRD and change its conformation should consequently activate Hh signaling. Currently, the only non-oxysterol small molecule known to bind SmoCRD is the plant alkaloid, cyclopamine (Nachtergaele et al., 2013). We obtained crystals of the XSmoCRD-cyclopamine complex and solved its structure at 2.5-Å resolution (Figures 4A and S5A; Table S1). Strikingly, in spite of the profound chemical differences between cyclopamine and 20(S)-OHC (Figure S1), cyclopamine-bound XSmoCRD adopts a structure almost identical to the XSmoCRD-20(S)-OHC complex (Figures 4B and S5B). We therefore tested if cyclopamine binding to CRD can activate Smo. However, cyclopamine also binds with high affinity to the 7TM small-molecule-binding site, causing Smo inhibition (Chen et al., 2002a). To determine the consequence of cyclopamine engaging only the CRD site, we generated the mutant mSmoD477G/E522K, which combines two point mutations that block cyclopamine binding to the 7TM site (Dijkgraaf et al., 2011; Yauch et al., 2009). Indeed, mSmoD477G/E522K did not bind the fluorescent derivative BODIPY-cyclopamine

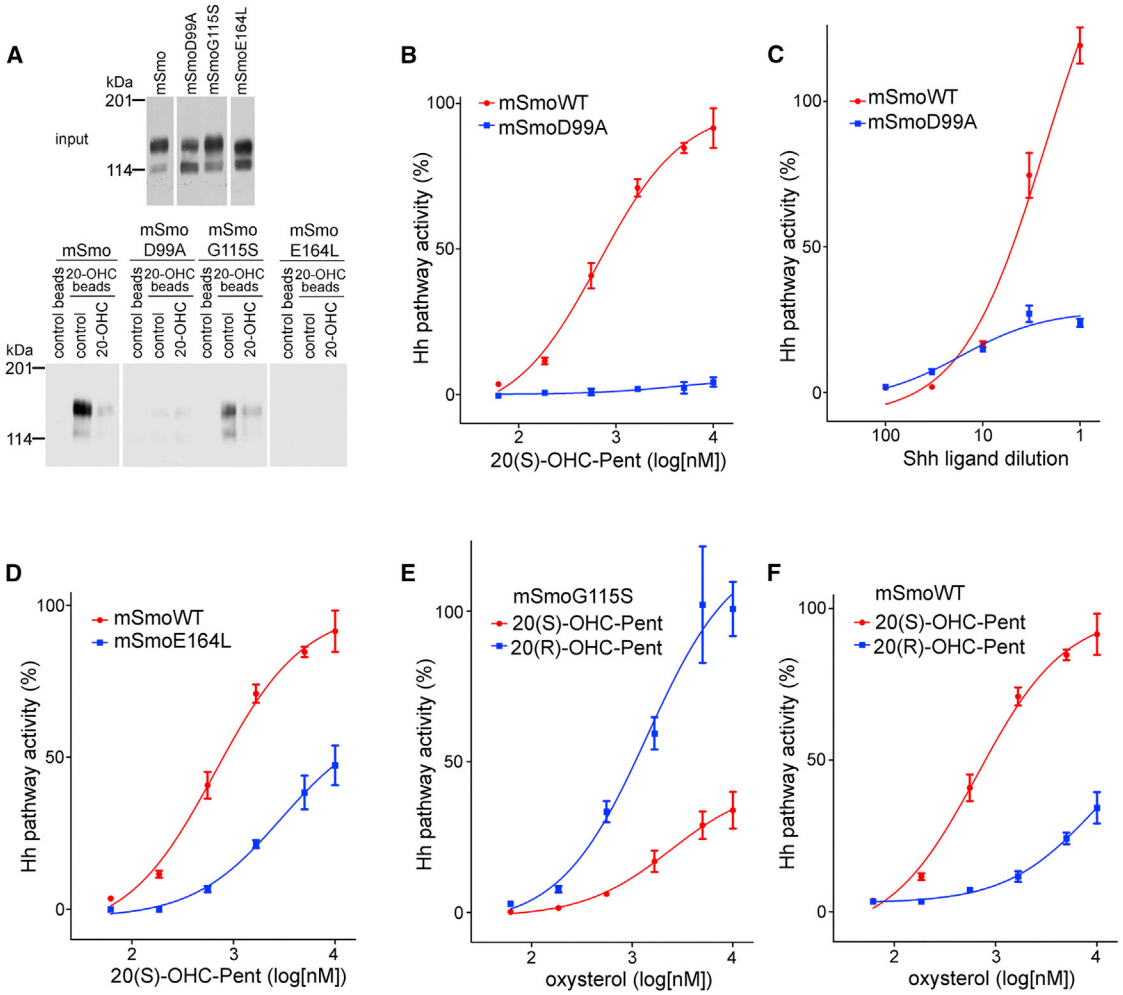

Figure 2. Oxysterol Recognition by Smo

(A) D99 and E164, the two mSmo residues that hydrogen bond with 3β-OH and 20(S)-OH, are critical for oxysterol binding. Full-length proteins expressed in 293T cells were assayed by binding to 20(S)-OHC affinity matrix (Nedelcu et al., 2013), in the absence or presence of free 20(S)-OHC competitor.

(B) Smo-null cells rescued with mSmoD99A do not respond to 20(S)-OHC-Pent, in contrast to cells rescued with wild-type mSmo. Hh pathway activity was assayed by qPCR for endogenous Gli1 and is shown normalized to activation elicited by saturating levels of SAG (0.5 μM). Error bars indicate SD (n = 3).

(C) As in (B), but treating cells with various concentrations of Shh. MSmoD99A does not respond to stimulation by Shh.

(D) As in (B), but with Smo-null cells rescued with mSmoE164L. The mutant has reduced responsiveness to oxysterols.

(E) mSmoG115S has reversed distereospecificity, responding stronger to 20(R)-OHC-Pent (EC_{50} = 1.3 μM) than to 20(S)-OHC-Pent (EC_{50} = 23.4 μM). See also oxysterol binding assays in Figure S3.

(F) In contrast, wild-type mSmo is activated preferentially by 20(S)-OHC-Pent (EC50=0.84 μM) compared to 20(R)-OHC-Pent (EC50=26.3 μM). Experiments in (B–F) were performed in parallel, and the curve for wild-type mSmo is shown in B, D and F.

(Figure S5C) and, furthermore, was not activated by SAG (Figure 4C), indicating that the 7TM small-molecule-binding site is broadly disabled by the two point mutations. Binding to oxysterols, however, was preserved in mSmoD477G/E522K (Figure S5D). Dramatically, cyclopamine activated mSmoD477G/E522K (Figure 4C), in contrast to cyclopamine inhibition of wild-type mSmo (Figure S5E). Importantly, mSmoD477G/E522K also retained activation by Shh and 20(S)-OHC (Figure 4C). These results suggest that ligand-induced conformational change in the CRD is sufficient to activate Smo, and that surprisingly, integrity of the 7TM small molecule-binding site of Smo is not necessary for Hh signaling.

Cholesterol Binds SmoCRD and Activates Hh Signaling

Although sterol binding to Smo is critical for Hh signaling, the endogenous sterol ligand remains unknown. Oxysterols, and in particular 20(S)-OHC, are unlikely candidates, being present endogenously at much lower levels than their EC_{50} for Hh pathway activation (Myers et al., 2013). We thus tested the possibility that cholesterol itself, by far the most abundant cellular sterol, might be the endogenous Smo ligand in vertebrate Hh signaling.

We first found that cholesterol binds SmoCRD, as demonstrated by the following results: (1) in a fluorescence polarization assay, cholesterol competed binding of BODIPY-cyclopamine

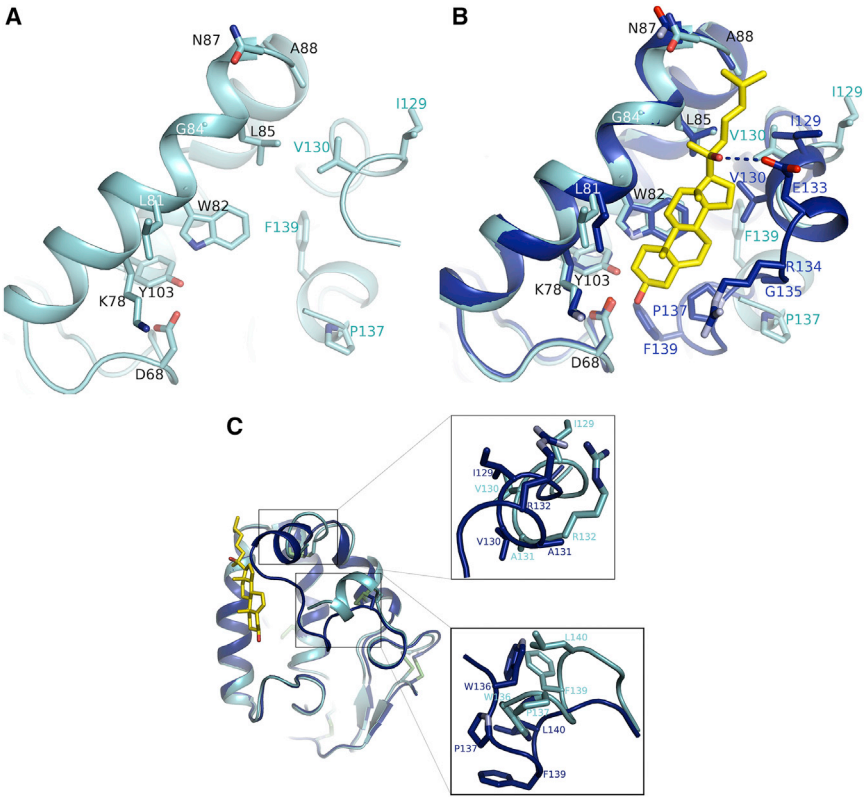

Figure 3. Sterol Binding Induces SmoCRD Conformational Change

(A) Close-up view of the sterol-binding site in unliganded XSmoCRD. The indicated amino acids are involved in sterol binding. See also Figure S4C for overall structure of unliganded XSmoCRD.

(B) As in (A), but with unliganded XSmoCRD (cyan) superimposed on 20(S)-OHC-bound XSmoCRD (navy). In absence of sterol, the binding site is in "open" state. 20(S)-OHC-induced conformational change results in "closed" state of the binding site.

(C) Ribbon diagram showing overall structure of unliganded XSmoCRD (cyan), superimposed on 20(S)-OHC-bound XSmoCRD (navy). Binding of 20(S)-OHC (yellow) induces inward rotation of helix H3′ (top right) and dramatic positional swap of residues in following loop (bottom right). See also Figure S4D for view from different angle.

to XSmo ectodomain (Figure 5A), with an apparent IC_{50} of 2.4 μM, which is within the range of physiological cholesterol concentration (Xie et al., 1999); (2) cholesterol enhanced the thermal stability of XSmo ectodomain in a circular dichroism (CD) melting assay (Figure S6A), indicative of binding—this effect was similar to the thermostabilizing effect of known CRD-binding molecules like 20(S)-OHC and cyclopamine (Figure S6B); and (3) we generated a novel cholesterol affinity resin, in which the sterol moiety is attached to beads via a C-19 handle (Figure S6C). This resin bound XSmo ectodomain specifically (Figure S6D), demonstrating that the structural elements of cholesterol are sufficient for Smo binding, while any sterol hydroxylation or oxidation is not necessary. In all these binding experiments, the closely related analog, cholestanol (Figure S1), was inactive, indicating the high specificity of SmoCRD for cholesterol.

Furthermore, exogenously added cholesterol activated Hh signaling in a dose-dependent manner (Figure 5B), suggesting that cholesterol binding is sufficient to activate Smo; as expected, cholestanol was inactive. Smo activation by cholesterol occurred via binding to the CRD, as it was drastically reduced by the D99A mutation (Figure S7A).

During vertebrate Hh signaling, Shh inhibits Ptch1, leading to Smo activation. If cholesterol were the endogenous Smo-activating ligand antagonized by Ptch1, one prediction is that cholesterol should display synergy with Shh. Indeed, low doses of Shh synergized with cholesterol in activating Hh signaling (Figure 5C), and conversely, low doses of cholesterol, but not cholestanol, displayed synergy with Shh (Figure S7B). Importantly, in agreement with previous reports (Nachtergaele et al., 2012), Shh did not synergize with 20(S)-OHC-Pent (Figure 5D). These results are consistent with cholesterol, but not the oxysterol, being the endogenous Smo ligand. We speculate that that the lack of synergy between Shh and 20(S)-OHC indicates that oxysterols cannot be inhibited by Ptch1, while cholesterol can.

Cholesterol as Endogenous Smo Activator

We used mutagenesis based on our XSmoCRD-20(S)-OHC structure to further demonstrate that cholesterol and not 20(S)-OHC is the endogenous ligand for Smo. To generate Smo mutants that distinguish between cholesterol and 20(S)-OHC, we focused on mSmo residues G115 and E164, which flank C-20 of the sterol molecule. The mutants, mSmoG115F, mSmoG115S, and mSmoG115S/E164L have abolished or significantly reduced responsiveness to 20(S)-OHC-Pent (Figures 6A and S7C). Strikingly, these mutants retain responsiveness to cholesterol (Figures 6B and S7D) as well as to Shh (Figures 6C and S7E). These results demonstrate that 20(S)-OHC is not required for Hh signaling and are consistent with cholesterol activating Smo during Shh stimulation.

We also asked whether the other oxysterols that can activate Smo, 25-OHC, 7-keto-25-OHC, and 7-keto-27-OHC (Figure S1), are required for Hh signaling. To address this question, we used a strategy based on the fluorinated cholesterol derivatives, 25-fluorocholesterol and F7-cholesterol (Carroll et al., 1998) (Figure S1). Since C-F bonds cannot be oxidized in cells, 25-fluorocholesterol cannot be converted into C-25-hydroxylated oxysterols (25-OHC and 7-keto-25-OHC), while F7-cholesterol cannot form oxysterols bearing C-25, C26, or C-27 hydroxyl groups (25-OHC, 7-keto-25-OHC, and 7-keto-27-OHC) (Carroll et al., 1998). Cells were depleted of sterols by incubation with

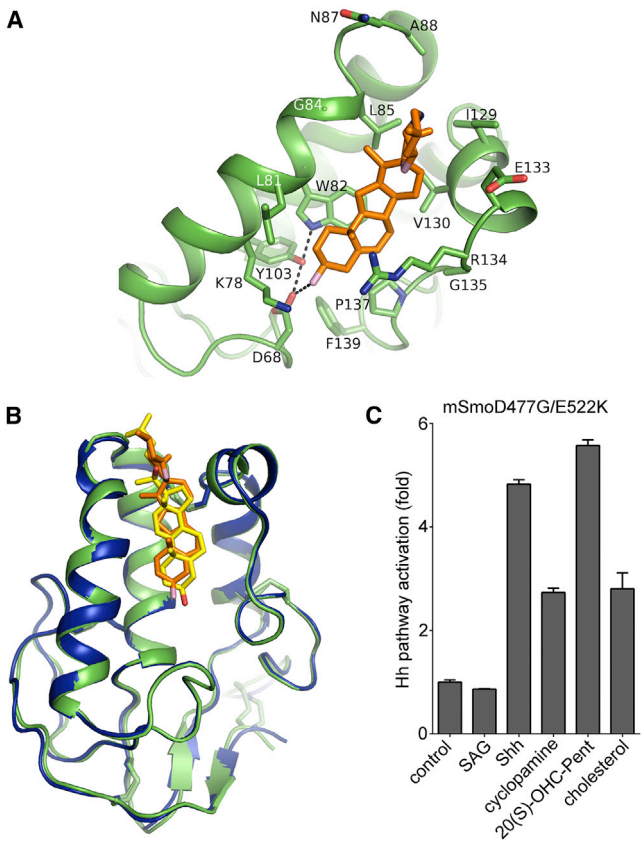

Figure 4. Sterol-Induced Conformational Change Activates Smo

(A) Cyclopamine bound in XSmoCRD sterol-binding site. Cyclopamine OH group is recognized by the same network of hydrogen bonds (dashed lines) as 3β-OH group of 20(S)-OHC. See also Figure S5A for overall structure.

(B) Superimposition of cyclopamine-bound (green) and 20(S)-OHC-bound (navy) XSmoCRD. Cyclopamine (orange) induces a protein conformation very similar to that induced by 20(S)-OHC (yellow). See also Figure S5B for a close-up view of binding site.

(C) Cyclopamine (100 μM, as soluble complex with methyl-β-cyclodextrin [MCD]) binding to CRD activates mSmoD477G/E522K, a mutant in which the cyclopamine-binding site in 7TM is destroyed. MSmoD477G/E522K also responds to 20(S)-OHC-Pent (10 μM), cholesterol (250 μM, as MCD complex), and Shh, but not SAG (0.5 μM), which binds the 7TM site. Error bars indicate SD (n = 3).

methyl-β-cyclodextrin (MCD), after which fluorinated sterols were added back as soluble MCD complexes, and the cells were stimulated with Shh, followed by assaying two Hh pathway readouts: recruitment of endogenous Smo to primary cilia (Corbit et al., 2005) and Hh transcriptional reporter assays. As expected, sterol depletion blocked Smo recruitment to cilia (Figures 6D and 6E) and Hh pathway activation (Figure 6F), which was rescued by pure cholesterol, but not by cholestanol. Interestingly, 25-fluorocholesterol completely rescued Hh signaling in sterol-depleted cells (Figures 6D–6F). Furthermore, F7-cholesterol showed significant rescue, although less than pure cholesterol (Figures 6D–6F). We speculate that the lower activity of F7-cholesterol is due to its reduced solubility compared to cholesterol and 25-fluorocholesterol. Together, these results demonstrate that cholesterol hydroxylation on C-25, C-26, or C-27 is not absolutely required for Hh signaling, indicating that 25-OHC, 7-keto-25-OHC, or 7-keto-27-OHC are not essential for Smo activation.

Recently, based on experiments showing that mSmoΔCRD is inhibited by sterol depletion, it was proposed that Smo contains an additional sterol-binding site, distinct from CRD (Myers et al., 2013). To elucidate which site mediates the effect of sterols on Smo, we compared the consequences of sterol depletion on mSmo and mSmoΔCRD activity (Figure 6G). Both mSmo and mSmoΔCRD activated Hh signaling; however, in contrast to mSmo, mSmoΔCRD activity was unaffected by sterol depletion (Figure 6G), indicating that sterols exert their effect on mSmo via the CRD and that basal activity of mSmoΔCRD is independent of sterols. We also measured ciliary localization of mSmo and mSmoΔCRD in response to Shh and to sterol depletion (Figure 6H). As expected, sterol depletion blocked mSmo recruitment to cilia in response to Shh; in contrast, ciliary localization of mSmoΔCRD was unaffected by either Shh or by sterol depletion (Figure 6H). This suggests that CRD is required for Smo regulation both by Shh and by sterols. Finally, we examined whether sterols are required for direct activation of Smo by SAG. Contrary to recent reports (Myers et al., 2013), we find that sterol depletion has no effect on Hh signaling triggered by SAG in Smo-null cells rescued with mSmo or with mSmoΔCRD (Figures 6G and 6H) or in wild-type NIH 3T3 cells (Figure 6I). Thus, Smo requires sterols for activation only during Shh stimulation, while sterols are no longer required when Smo is forced into active conformation by the SAG agonist.

Discussion

Smo is essential for relaying Hh signals across plasma membrane. In absence of stimulation, Ptch represses Smo, ensuring that Hh pathway is inhibited. Signaling is triggered by Hh ligand, which inhibits Ptch, thus allowing Smo to adopt an active conformation and transduce Hh signals to the cytoplasm. A critical unanswered question has been how Smo is regulated. As 7TM protein targeted by numerous synthetic agonists and antagonists, Smo was postulated be controlled by an unidentified endogenous ligand. This hypothesis is also consistent with Ptch belonging to the RND family of small molecule pumps, suggesting that the Smo ligand is itself regulated by Ptch. Sterol depletion inhibits vertebrate Smo, and furthermore, some oxysterols activate Smo by binding to its CRD; together, these findings suggested that Smo is regulated by a sterol activator. However, the identity of the endogenous sterol has remained unknown, as well as how Smo recognizes sterols and how sterols activate Smo.

Here, we first elucidate how Smo recognizes sterols, by solving the crystal structure of SmoCRD in complex with 20(S)-OHC. We then use structure-guided mutagenesis to demonstrate that sterol binding is critical for Smo activation by upstream Shh signaling through Ptch1, as well as to explain the basis for diastereospecific Smo activation by oxysterols. Next, we solve the structure of SmoCRD alone, revealing that sterol binding triggers a conformational change. We also determine the structure of SmoCRD in complex with the plant alkaloid, cyclopamine, which shows a conformation almost identical to that of

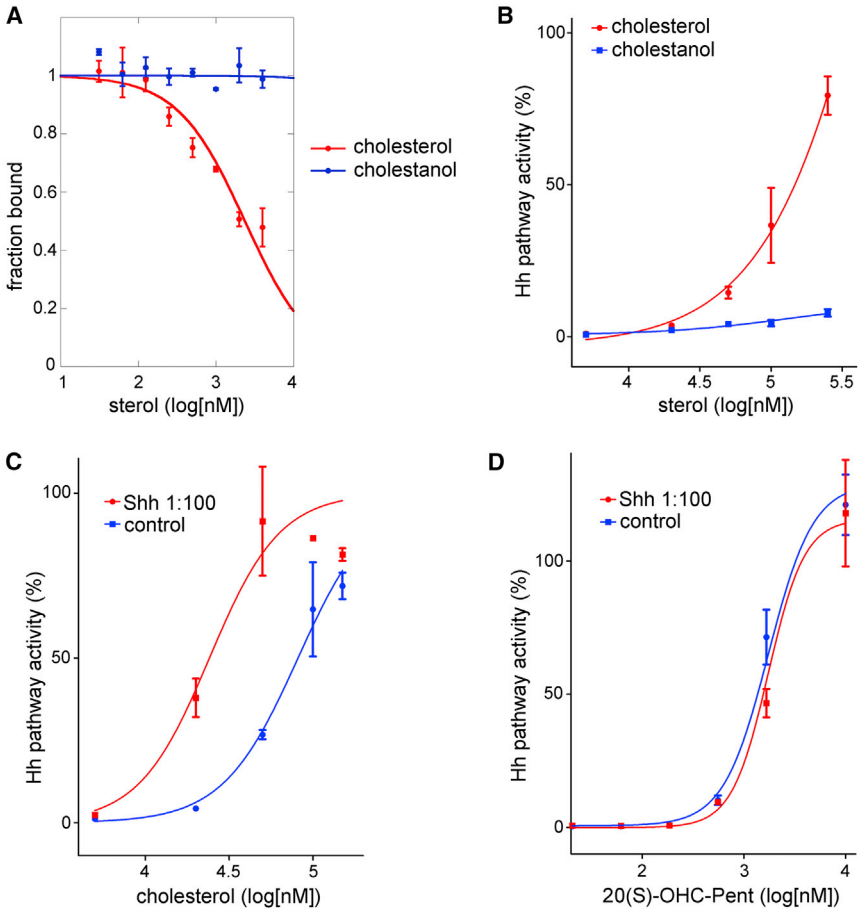

Figure 5. Cholesterol Binds Smo and Activates Hh Signaling

(A) Fluorescence polarization assay showing cholesterol competes binding of BODIPY-cyclopamine to purified XSmo ectodomain in dose-dependent manner (IC_{50} = 2.4 μM). In contrast, the saturated analog cholestanol, does not bind Smo. See also Figure S6 for additional assays demonstrating binding of cholesterol to XSmoCRD.

(B) Cholesterol, but not cholestanol, activates Hh signaling in Smo-null cells rescued with wild-type mSmo. Cholesterol and cholestanol were delivered as MCD complexes. Error bars indicate SD (n = 3).

(C) Cholesterol (added as MCD complex) synergizes with Shh to activate Hh signaling in NIH 3T3 cells. See also Figure S7B showing synergy of Shh with cholesterol, but not cholestanol. Error bars indicate SD (n = 3).

(D) Unlike cholesterol, the oxysterol 20(S)-OHC-Pent does not synergize with Shh in NIH 3T3 cells.

oxysterol-bound SmoCRD: we exploit this similarity to show that CRD conformational change is sufficient to activate Smo, suggesting that it is a key event in allosteric Smo activation. Importantly, we discover that cholesterol itself binds and activates Smo, as well as synergizes with Shh. Furthermore, we demonstrate that the known Smo-activating oxysterols are not required for Smo activation in cells. Taken together, our data support a model in which cholesterol is the endogenous ligand responsible for Smo activation during Hh signaling, and that Ptch1 inhibits Smo by counteracting its activation by cholesterol (Figure 7). Thus cholesterol plays a unique role as second messenger in vertebrate Hh signaling, mediating the functional interaction between Ptch1 and Smo.

Our structural analysis clarifies how Smo recognizes, and how it is activated by, sterols. We show that sterols occupy their site on SmoCRD in a head-to-tail orientation that matches that of the palmitoyl residue of Wnt8 binding to Fz8CRD (Janda et al., 2012), thus disproving the previous model based on molecular docking of 20(S)-OHC to unliganded zfSmoCRD (Nachtergaele et al., 2013). Reminiscent of steroid hormone receptors, SmoCRD discriminates sterols from other lipids by exploiting both shape and amphipathic properties. The high degree of shape complementarity between SmoCRD and 20(S)-OHC suggests that the endogenous ligand for Smo is indeed a sterol: this notion is further supported by the fact that recognition of 3β-OH, a universally conserved feature of sterols, is essential for both Smo-sterol interaction and for Smo activation by Shh. Based on the SmoCRD-20(S)-OHC structure, we also elucidate the basis for diastereoselective recognition of 20(S)-OHC and validate our model by generating a Smo mutant that responds to 20(R)-OHC instead of 20(S)-OHC. Our data also highlights the exquisite sterol specificity of Smo, which discriminates between cholesterol and the reduced analog, cholestanol. Interestingly, while Smo does not bind cholestanol, we have shown that it binds a C-20(S)-hydroxylated derivative of it (Nedelcu et al., 2013). Perhaps, hydrogen bonding between 20(S)-OH and the conserved E164 in mSmo is able to rescue cholestanol binding to Smo.

Unexpectedly, sterol binding to SmoCRD triggers a conformational change, suggesting a mechanism for Smo activation. Interestingly, such a ligand-induced conformational change has not been seen in other CRDs. In the case of the related Fz8 receptor, Wnt8 binding does not change Fz8CRD conformation (Janda et al., 2012): this is consistent with Wnt-Fz interaction alone not being sufficient for downstream pathway activation, which requires recruitment of co-receptors, such as lipoprotein-receptor-related protein (LRP)-5/6 in the canonical pathway or tyrosine kinase receptor ROR2 in the non-canonical pathway. Together, these differences suggest that Smo and Fz proteins have evolved distinct activation mechanisms.

How does oxysterol binding to SmoCRD activate the rest of the protein? A likely possibility is that it occurs through communication with the extracellular loops (ECLs) of the 7TM domain of Smo (Wang et al., 2013), from which conformational change propagates to, and activates, the parts of Smo facing the cytosol. We speculate that CRD, ECLs, and TM helices form an integrated multi-domain convergence zone, in which ECLs mediate communication between CRD and 7TM: this model is

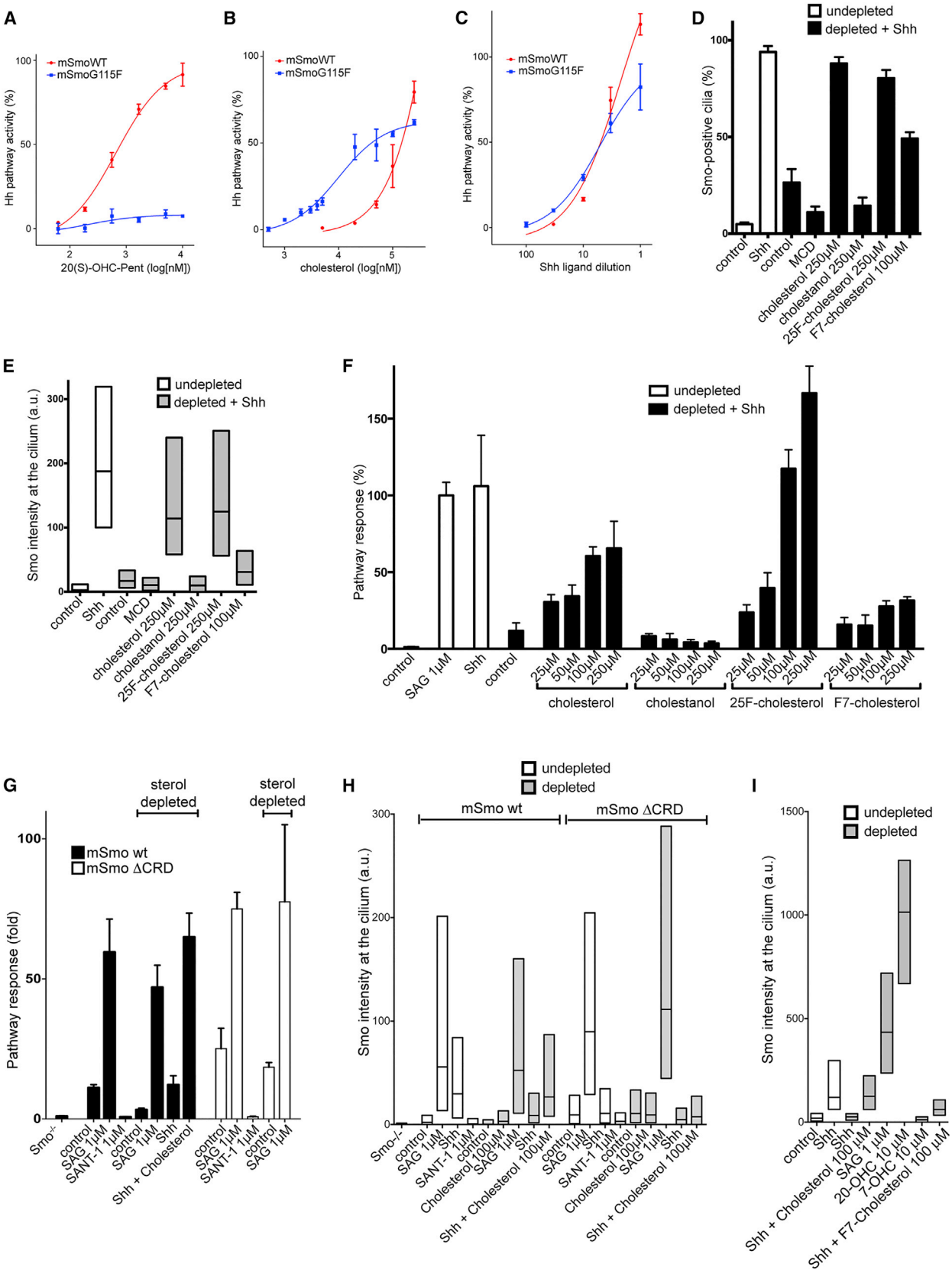

(legend on next page)

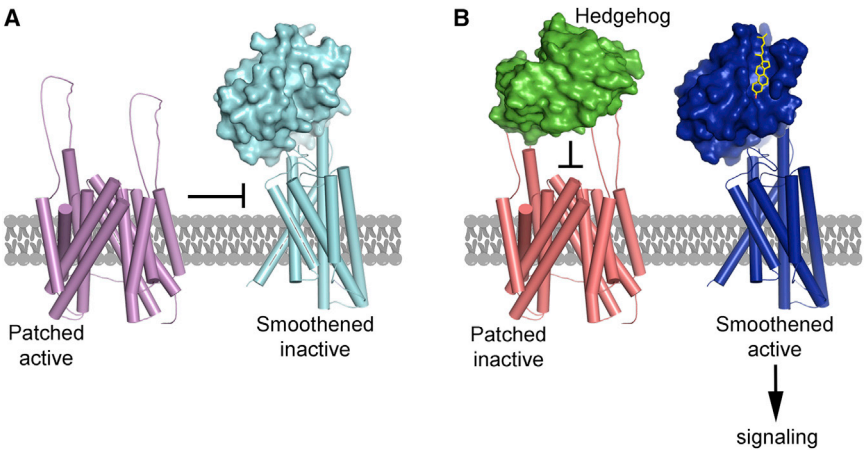

Figure 7. Model for Smo Regulation During Vertebrate Hh Signaling

(A) In the absence of Hh signaling, active Ptch1 maintains Smo inhibited, with its CRD sterol-binding site empty.

(B) Upon Shh binding, Ptch1 is inhibited, and cholesterol (yellow) gains access to SmoCRD. Cholesterol-induced conformational change in CRD causes allosteric activation of the 7TM domain of Smo, which in turn, signals to the cytoplasm. These events occur in primary cilia of vertebrate cells. For simplicity, other ciliary proteins required for Smo signaling, such as Evc proteins (Dorn et al., 2012), are not shown.

reminiscent of the communication between activator-bound allosteric site and agonist-bound orthosteric site observed in the recent M2 muscarinic acetylcholine receptor structure (Kruse et al., 2013). Interestingly, the extracellular region of M2 receptor also adopts a contracted shape upon allosteric ligand capture, similar to the change in SmoCRD induced by sterol binding. Ultimately, structure of full-length Smo, as well as mechanistic studies, will be needed to decipher how sterol binding to CRD activates Smo.

The small-molecule-binding site in the 7TM domain of Smo (Chen et al., 2002a; Wang et al., 2013) was the first one identified, followed by the sterol-binding site in CRD (Myers et al., 2013; Nachtergaele et al., 2013; Nedelcu et al., 2013). Unlike the CRD site, however, no endogenous metabolite has been found to bind the 7TM site. Furthermore, mutations that broadly impair binding of exogenous small molecules to the 7TM site, do not affect Smo activation by Shh; in contrast, blocking sterol binding to the CRD site abolishes Smo activation by Shh. We speculate that, while the 7TM site is of great importance as a drug target, it may not interact with an endogenous Smo ligand. It remains possible, however, that in some contexts, unidentified metabolites modulate Smo via 7TM site.

Oxysterols have been the only known metabolites that activate Hh signaling, although it is unclear if they are present in cells in sufficient amounts to activate Smo. The most potent oxysterol is 20(S)-OHC, but three other oxysterols, 25-OHC, 7-keto-25-OHC, and 7-keto-27-OHC, also activate Smo. We address the issue of whether these oxysterols are required for Hh signaling, which has remained an open question. We find that cholesterol analogs fluorinated at C-25, C-26, and C-27 rescue Hh signaling in sterol-depleted cells, indicating that 25-OHC, 7-keto-25-OHC, and 7-keto-27-OHC are not absolutely required for Hh signaling.

Figure 6. Evidence that Cholesterol Is Endogenous Activator of Smo in Vertebrate Hh Signaling

(A) 20(S)-OHC-Pent does not activate Hh signaling in Smo-null cells rescued with mSmoG115F. Error bars indicate SD (n = 3). This experiment was performed in parallel with the one in Figure 2B, having the same curve for wild-type mSmo. See Figure S7C for similar behavior of mSmoG115S and mSmoG115S/E164L.

(B) In contrast, Smo-null cells rescued with mSmoG115F respond to cholesterol. This experiment was performed in parallel with the one in Figure 5B, and shows the same curve for wild-type mSmo stimulation by cholesterol. See Figure S7D for similar behavior of mSmoG115S and mSmoG115S/E164L.

(C) MSmoG115F also responds to Shh. This experiment was performed in parallel with the experiment in Figure 2C, and shows the same curve for wild-type mSmo. See Figure S7E for similar behavior of mSmoG115S and mSmoG115S/E164L.

(D) The indicated sterols (see Figure S1 for structures) were added back as MCD complexes to sterol-depleted NIH 3T3 cells, followed by incubation with Shh. Hh signaling was assayed by measuring ciliary recruitment of endogenous Smo. The graph shows fraction of Smo-positive cilia. Sterol depletion blocks Smo recruitment to cilia in response to Shh, which is rescued by cholesterol, 25F-cholesterol, and F7-cholesterol, but not by cholestanol. The MCD control shows effect of adding empty MCD instead of MCD-sterol. Between 300 and 600 cilia were measured per condition.

(E) As in (D), but Smo intensity at cilia is displayed as boxplots representing the distribution between 25th and 75th percentile, with horizontal line indicating median intensity.

(F) As in (D), but Hh signaling was measured by luciferase reporter assay in Shh Light II cells. Error bars indicate SD (n = 4). Hh signaling in sterol-depleted cells is rescued by cholesterol, 25F-cholesterol, and F7-cholesterol, but not by cholestanol. Cholesterol hydroxylation at C-25 or C-27 is thus not absolutely required for Hh signaling.

(G) Smo-null cells, rescued with mSmo or mSmoΔCRD, were sterol-depleted, followed by incubation with indicated agents. Hh pathway activity was measured by qPCR for Gli1 mRNA. Error bars indicate SD (n = 3). Signaling by mSmoΔCRD is not inhibited by sterol depletion, in contrast to mSmo. Both mSmo and mSmoΔCRD are inhibited by SANT1 and are activated by SAG, irrespective of sterol depletion. Cholesterol add-back (100 μM MCD complex) rescues mSmo activation by Shh, demonstrating efficiency of sterol depletion.

(H) As in (G), but measuring ciliary localization of mSmo and mSmoΔCRD. Shh recruits mSmo to cilia in sterol-dependent manner; in contrast, Shh has no effect on ciliary levels of mSmoΔCRD. Both mSmo and mSmoΔCRD accumulate in cilia in response to SAG, which is unaffected by sterol depletion. Ciliary levels of both proteins are reduced by SANT1. ≥300 cilia were measured per condition.

(I) Ciliary localization of endogenous Smo was measured in sterol-depleted NIH 3T3 cells, as in (E). SAG and 20-OHC strongly recruit Smo to cilia in sterol-depleted cells, in contrast to Shh. The inactive oxysterol, 7-hydroxycholesterol (7-OHC), serves as negative control. Between 80 and 140 cilia were measured per condition.

Furthermore, 20(S)-OHC is also not required for Hh signaling, as shown by mutants such as mSmoG115F, which does not respond to 20(S)-OHC, but is still activated by Shh.

We find that cholesterol fulfills the criteria for being the endogenous Smo ligand. Cholesterol binds SmoCRD with micromolar affinity, within the range of endogenous cholesterol levels (Xie et al., 1999). We note that affinity for cholesterol might be higher for full-length Smo, as other domains of the protein might cooperate to enhance binding, possibly by shielding the β face of the sterol molecule, which is not engaged in CRD binding. Cholesterol also activates Smo, including mutants that do not respond to 20(S)-OHC, like mSmoG115F. Furthermore, cholesterol synergizes with Shh to activate Smo, as expected for an endogenous Smo ligand that is negatively regulated by Ptch1. In contrast to cholesterol, 20(S)-OHC does not synergize with Shh. We speculate that this difference is due to Ptch1 inability to inhibit 20(S)-OHC. Perhaps Ptch1 antagonizes cholesterol at the membrane bilayer level, and 20(S)-OHC, by virtue of its much higher water solubility compared to cholesterol, can escape inhibition by Ptch1.

Our results also clarify the role of CRD in Smo regulation. In contrast to a recent report (Myers et al., 2013), we find that sterol depletion does not block activation of Hh signaling by SmoΔCRD, or by SAG: this demonstrates that CRD mediates the effect of sterols on Smo and that Smo requires sterols only when activated by upstream Shh, while SAG, by directly activating Smo, bypasses the sterol requirement. We also find that SmoΔCRD levels in cilia are not affected by Shh, suggesting that CRD is critical for Smo regulation by Shh-Ptch1: this view is consistent with results showing that SmoΔCRD is not responsive to Shh (Aanstad et al., 2009) and that replacing CRD and the first two TM domains of Smo with corresponding portions of Fz5, results in a protein no longer inhibited by Ptch1 (Murone et al., 1999). We have previously observed a small effect of Shh on overexpressed SmoΔCRD in qPCR assays (Nedelcu et al., 2013), so it is possible that SmoΔCRD retains some residual regulation by Ptch1.

How does Ptch1 inhibit Smo? Since Ptch1 acts at the primary cilium (Rohatgi et al., 2007), a possibility is that Ptch1 maintains low levels and/or chemical activity of cholesterol in the ciliary membrane, thereby ensuring that Smo will not be activated. Upon Ptch1 inhibition by Shh, cholesterol activity in cilia increases, leading to Smo activation: testing this hypothesis will require developing methods to image cholesterol in cilia. In this model, Smo arrives at cilia in an unliganded, inactive form. Perhaps cholesterol activity in compartments through which Smo traffics on its way to the cilium is too low for binding to Smo. Alternatively, Smo binds cholesterol before reaching the cilium, but the low cholesterol maintained by Ptch1 in cilia favors dissociation, thereby inhibiting Smo. Importantly, ciliary resident proteins that interact with Smo, such as EVC proteins, are required for turning on signaling downstream of Smo (Dorn et al., 2012): this ensures that, even if cholesterol binds Smo and induces it to adopt an active conformation outside the cilium, this will not trigger Hh signal transduction. A detailed analysis of where the interaction between Smo and cholesterol takes place in the cell will be needed to answer these questions, as well as determining if and how Ptch1 regulates cholesterol in cilia.

STAR★METHODS

Detailed methods are provided in the online version of this paper and include the following:

- KEY RESOURCES TABLE
- CONTACT FOR REAGENT AND RESOURCE SHARING
- EXPERIMENTAL MODEL AND SUBJECT DETAILS
  - Cell Culture and Generation of Stable Cell Lines
- METHOD DETAILS
  - Reagents
  - Antibodies
  - Hh Pathway Assays
  - Sterol Depletion and Rescue Experiments
  - Immunofluorescence and Measurements of Smo Ciliary Localization
  - BODIPY-Cyclopamine Binding Assays
  - Sterol Affinity Matrices
  - Sterol Affinity Assays
  - Recombinant Protein Expression and Purification
  - Crystallization, Data Collection, and Structure Determination
  - Fluorescence Polarization-Based Ligand Binding Assays
  - Circular Dichroism Temperature Melting Experiments
  - Chemical Synthesis
- QUANTIFICATION AND STATISTICAL ANALYSIS
- DATA AND SOFTWARE AVAILABILITY
  - Data Resources

SUPPLEMENTAL INFORMATION

Supplemental Information includes seven figures, two tables, and one movie and can be found with this article at http://dx.doi.org/10.1016/j.cell.2016.08.003.

AUTHOR CONTRIBUTIONS

P.H., D.N., M.W., and A.S. performed cellular and biochemical experiments. J.L. synthesized, purified, and characterized BODIPY probes. C.J. synthesized, purified, and characterized the C19-position cholesterol analog. Y.K. collected diffraction data sets. P.H. solved the structures. P.H., D.N., M.W., and A.S. analyzed data. A.S. and P.H. wrote the manuscript, with input from the other authors.

ACKNOWLEDGMENTS

This work was supported by NIH grants RO1 GM092924 and GM110041 to A.S. We thank members of the Salic lab for helpful discussions and members of the Structural Biology Center at Argonne National Laboratory for help with data collection at the 19-ID beam line.

Received: April 23, 2016
Revised: June 14, 2016
Accepted: July 30, 2016
Published: August 18, 2016

REFERENCES

Aanstad, P., Santos, N., Corbit, K.C., Scherz, P.J., Trinh, A., Salvenmoser, W., Huisken, J., Reiter, J.F., and Stainier, D.Y. (2009). The extracellular domain of

Smoothened regulates ciliary localization and is required for high-level Hh signaling. Curr. Biol. *19*, 1034–1039.

Alcedo, J., Ayzenzon, M., Von Ohlen, T., Noll, M., and Hooper, J.E. (1996). The Drosophila smoothened gene encodes a seven-pass membrane protein, a putative receptor for the hedgehog signal. Cell *86*, 221–232.

Bazan, J.F., and de Sauvage, F.J. (2009). Structural ties between cholesterol transport and morphogen signaling. Cell *138*, 1055–1056.

Braberg, H., Webb, B.M., Tjioe, E., Pieper, U., Sali, A., and Madhusudhan, M.S. (2012). SALIGN: a web server for alignment of multiple protein sequences and structures. Bioinformatics *28*, 2072–2073.

Carroll, J.N., Pinkerton, F.D., Su, X., Gerst, N., Wilson, W.K., and Schroepfer, G.J., Jr. (1998). Sterol synthesis. Synthesis of 3 beta-hydroxy-25,26,26,26,27,27,27-heptafluorocholest-5-en-7-one and its effects on HMG-CoA reductase activity in Chinese hamster ovary cells, on ACAT activity in rat jejunal microsomes, and serum cholesterol levels in rats. Chem. Phys. Lipids *94*, 209–225.

Chen, J.K., Taipale, J., Cooper, M.K., and Beachy, P.A. (2002a). Inhibition of Hedgehog signaling by direct binding of cyclopamine to Smoothened. Genes Dev. *16*, 2743–2748.

Chen, J.K., Taipale, J., Young, K.E., Maiti, T., and Beachy, P.A. (2002b). Small molecule modulation of Smoothened activity. Proc. Natl. Acad. Sci. USA *99*, 14071–14076.

Cooper, M.K., Wassif, C.A., Krakowiak, P.A., Taipale, J., Gong, R., Kelley, R.I., Porter, F.D., and Beachy, P.A. (2003). A defective response to Hedgehog signaling in disorders of cholesterol biosynthesis. Nat. Genet. *33*, 508–513.

Corbit, K.C., Aanstad, P., Singla, V., Norman, A.R., Stainier, D.Y., and Reiter, J.F. (2005). Vertebrate Smoothened functions at the primary cilium. Nature *437*, 1018–1021.

Corcoran, R.B., and Scott, M.P. (2006). Oxysterols stimulate Sonic hedgehog signal transduction and proliferation of medulloblastoma cells. Proc. Natl. Acad. Sci. USA *103*, 8408–8413.

Dijkgraaf, G.J., Alicke, B., Weinmann, L., Januario, T., West, K., Modrusan, Z., Burdick, D., Goldsmith, R., Robarge, K., Sutherlin, D., et al. (2011). Small molecule inhibition of GDC-0449 refractory smoothened mutants and downstream mechanisms of drug resistance. Cancer Res. *71*, 435–444.

Dorn, K.V., Hughes, C.E., and Rohatgi, R. (2012). A Smoothened-Evc2 complex transduces the Hedgehog signal at primary cilia. Dev. Cell *23*, 823–835.

Dwyer, J.R., Sever, N., Carlson, M., Nelson, S.F., Beachy, P.A., and Parhami, F. (2007). Oxysterols are novel activators of the hedgehog signaling pathway in pluripotent mesenchymal cells. J. Biol. Chem. *282*, 8959–8968.

Emsley, P., and Cowtan, K. (2004). Coot: model-building tools for molecular graphics. Acta Crystallogr. D Biol. Crystallogr. *60*, 2126–2132.

Frank-Kamenetsky, M., Zhang, X.M., Bottega, S., Guicherit, O., Wichterle, H., Dudek, H., Bumcrot, D., Wang, F.Y., Jones, S., Shulok, J., et al. (2002). Small-molecule modulators of Hedgehog signaling: identification and characterization of Smoothened agonists and antagonists. J. Biol. *1*, 10.

Gimpl, G., Klein, U., Reiländer, H., and Fahrenholz, F. (1995). Expression of the human oxytocin receptor in baculovirus-infected insect cells: high-affinity binding is induced by a cholesterol-cyclodextrin complex. Biochemistry *34*, 13794–13801.

Greenfield, N.J. (2006). Using circular dichroism spectra to estimate protein secondary structure. Nat. Protoc. *1*, 2876–2890.

Ingham, P.W., and McMahon, A.P. (2001). Hedgehog signaling in animal development: paradigms and principles. Genes Dev. *15*, 3059–3087.

Janda, C.Y., Waghray, D., Levin, A.M., Thomas, C., and Garcia, K.C. (2012). Structural basis of Wnt recognition by Frizzled. Science *337*, 59–64.

Jao, C.Y., Nedelcu, D., Lopez, L.V., Samarakoon, T.N., Welti, R., and Salic, A. (2015). Bioorthogonal probes for imaging sterols in cells. ChemBioChem *16*, 611–617.

Kim, W.K., Meliton, V., Amantea, C.M., Hahn, T.J., and Parhami, F. (2007). 20(S)-hydroxycholesterol inhibits PPARgamma expression and adipogenic differentiation of bone marrow stromal cells through a hedgehog-dependent mechanism. J. Bone Miner. Res. *22*, 1711–1719.

Kruse, A.C., Ring, A.M., Manglik, A., Hu, J., Hu, K., Eitel, K., Hübner, H., Pardon, E., Valant, C., Sexton, P.M., et al. (2013). Activation and allosteric modulation of a muscarinic acetylcholine receptor. Nature *504*, 101–106.

Lum, L., and Beachy, P.A. (2004). The Hedgehog response network: sensors, switches, and routers. Science *304*, 1755–1759.

McCoy, A.J., Grosse-Kunstleve, R.W., Adams, P.D., Winn, M.D., Storoni, L.C., and Read, R.J. (2007). Phaser crystallographic software. J. Appl. Cryst. *40*, 658–674.

Minor, W., Cymborowski, M., Otwinowski, Z., and Chruszcz, M. (2006). HKL-3000: the integration of data reduction and structure solution–from diffraction images to an initial model in minutes. Acta Crystallogr. D Biol. Crystallogr. *62*, 859–866.

Murakami, S., Nakashima, R., Yamashita, E., Matsumoto, T., and Yamaguchi, A. (2006). Crystal structures of a multidrug transporter reveal a functionally rotating mechanism. Nature *443*, 173–179.

Murone, M., Rosenthal, A., and de Sauvage, F.J. (1999). Sonic hedgehog signaling by the patched-smoothened receptor complex. Curr. Biol. *9*, 76–84.

Myers, B.R., Sever, N., Chong, Y.C., Kim, J., Belani, J.D., Rychnovsky, S., Bazan, J.F., and Beachy, P.A. (2013). Hedgehog pathway modulation by multiple lipid binding sites on the smoothened effector of signal response. Dev. Cell *26*, 346–357.

Nachtergaele, S., Mydock, L.K., Krishnan, K., Rammohan, J., Schlesinger, P.H., Covey, D.F., and Rohatgi, R. (2012). Oxysterols are allosteric activators of the oncoprotein Smoothened. Nat. Chem. Biol. *8*, 211–220.

Nachtergaele, S., Whalen, D.M., Mydock, L.K., Zhao, Z., Malinauskas, T., Krishnan, K., Ingham, P.W., Covey, D.F., Siebold, C., and Rohatgi, R. (2013). Structure and function of the Smoothened extracellular domain in vertebrate Hedgehog signaling. eLife *2*, e01340.

Nakano, Y., Guerrero, I., Hidalgo, A., Taylor, A., Whittle, J.R., and Ingham, P.W. (1989). A protein with several possible membrane-spanning domains encoded by the Drosophila segment polarity gene patched. Nature *341*, 508–513.

Nedelcu, D., Liu, J., Xu, Y., Jao, C., and Salic, A. (2013). Oxysterol binding to the extracellular domain of Smoothened in Hedgehog signaling. Nat. Chem. Biol. *9*, 557–564.

Rohatgi, R., Milenkovic, L., and Scott, M.P. (2007). Patched1 regulates hedgehog signaling at the primary cilium. Science *317*, 372–376.

Sinha, S., and Chen, J.K. (2006). Purmorphamine activates the Hedgehog pathway by targeting Smoothened. Nat. Chem. Biol. *2*, 29–30.

Taipale, J., Chen, J.K., Cooper, M.K., Wang, B., Mann, R.K., Milenkovic, L., Scott, M.P., and Beachy, P.A. (2000). Effects of oncogenic mutations in Smoothened and Patched can be reversed by cyclopamine. Nature *406*, 1005–1009.

Taipale, J., Cooper, M.K., Maiti, T., and Beachy, P.A. (2002). Patched acts catalytically to suppress the activity of Smoothened. Nature *418*, 892–897.

Tseng, T.T., Gratwick, K.S., Kollman, J., Park, D., Nies, D.H., Goffeau, A., and Saier, M.H., Jr. (1999). The RND permease superfamily: an ancient, ubiquitous and diverse family that includes human disease and development proteins. J. Mol. Microbiol. Biotechnol. *1*, 107–125.

Tukachinsky, H., Lopez, L.V., and Salic, A. (2010). A mechanism for vertebrate Hedgehog signaling: recruitment to cilia and dissociation of SuFu-Gli protein complexes. J. Cell Biol. *191*, 415–428.

Tukachinsky, H., Kuzmickas, R.P., Jao, C.Y., Liu, J., and Salic, A. (2012). Dispatched and scube mediate the efficient secretion of the cholesterol-modified hedgehog ligand. Cell Rep. *2*, 308–320.

van den Heuvel, M., and Ingham, P.W. (1996). smoothened encodes a receptor-like serpentine protein required for hedgehog signalling. Nature *382*, 547–551.

Voss, N.R., and Gerstein, M. (2010). 3V: cavity, channel and cleft volume calculator and extractor. Nucleic Acids Res. *38*, W555–W562.

Wang, C., Wu, H., Katritch, V., Han, G.W., Huang, X.P., Liu, W., Siu, F.Y., Roth, B.L., Cherezov, V., and Stevens, R.C. (2013). Structure of the human smoothened receptor bound to an antitumour agent. Nature *497*, 338–343.

Xie, C., Turley, S.D., and Dietschy, J.M. (1999). Cholesterol accumulation in tissues of the Niemann-pick type C mouse is determined by the rate of lipoprotein-cholesterol uptake through the coated-pit pathway in each organ. Proc. Natl. Acad. Sci. USA *96*, 11992–11997.

Yauch, R.L., Dijkgraaf, G.J., Alicke, B., Januario, T., Ahn, C.P., Holcomb, T., Pujara, K., Stinson, J., Callahan, C.A., Tang, T., et al. (2009). Smoothened mutation confers resistance to a Hedgehog pathway inhibitor in medulloblastoma. Science *326*, 572–574.

STAR★METHODS

KEY RESOURCES TABLE

REAGENT or RESOURCE	SOURCE	IDENTIFIER
Antibodies		
Rabbit anti-mCherry	Nedelcu et al., 2013	N/A
Rabbit anti-mouse Smo	Tukachinsky et al., 2010	N/A
Mouse anti-acetylated tubulin	Sigma	Cat# T7451; RRID: AB_609894
Chemicals, Peptides, and Recombinant Proteins		
SAG	Axxora	Cat# BV-1939
SANT1	Calbiochem	Cat# 559303
cyclopamine	LC Laboratories	Cat# C-8700
BODIPY-cyclopamine	TRC	Cat# B674800
20(S)-hydroxycholesterol	Steraloids	Cat# C6480-000
25-fluorocholesterol	Steraloids	Cat# C6688-000
20(S)-OHC-Pent and 20(R)-OHC-Pent	Nedelcu et al., 2013	N/A
Critical Commercial Assays		
Dual-Glo Luciferase assay system	Promega	Cat# E2920
Transcriptor reverse transcriptase	Roche	Cat# 03531287001
RNA-Bee reagent	TelTest	Cat# CS105B
RQ1 RNase-free DNase	Promega	Cat# M6101
FastStart SYBR Green Master reagent	Roche	Cat# 04673492001
Deposited Data		
Atomic coordinates, apo XSmoCRD structure	Protein Data Bank	PDB: 5KZZ
Atomic coordinates, XSmoCRD-20(S)-OHC structure	Protein Data Bank	PDB: 5KZV
Atomic coordinates, XSmoCRD-cyclopamine structure	Protein Data Bank	PDB: 5KZY
Experimental Models: Cell Lines		
NIH 3T3 cells	ATCC	Cat# CRL1658
Immortalized Smo−/− mouse embryonic fibroblasts	Nedelcu et al., 2013	N/A
Recombinant DNA		
pCS2-mSmo-mCherry	Nedelcu et al., 2013	N/A
pCS2-mSmoDCRD-mCherry	Nedelcu et al., 2013	N/A
pCS2-mSmo-mCherry, various point mutants	This paper	N/A
pET32-XSmoCRD	This paper	N/A
pET32-XSmo ectodomain	This paper	N/A
Sequence-Based Reagents		
L27 forward primer: 5′-GTCGAGATGGGCAAGTTCAT-3′	Nedelcu et al., 2013	N/A
L27 reverse primer: 5′-GCTTGGCGATCTTCTTCTTG-3′	Nedelcu et al., 2013	N/A
Gli1 forward primer: 5′-GGCCAATCACAAGTCAAGGT-3′	Nedelcu et al., 2013	N/A
Gli1 forward primer: 5′-TTCAGGAGGAGGGTACAACG −3′	Nedelcu et al., 2013	N/A
Software and Algorithms		
Metamorph image acquisition software	Applied Precision	N/A
HKL-3000	Minor et al., 2006	N/A
PHASER	McCoy et al., 2007	N/A
COOT	Emsley and Cowtan, 2004	N/A
Prism 5	GraphPad	www.graphpad.com

CONTACT FOR REAGENT AND RESOURCE SHARING

Further information and requests for reagents may be directed to, and will be fulfilled by the corresponding author Adrian Salic (asalic@hms.harvard.edu).

EXPERIMENTAL MODEL AND SUBJECT DETAILS

Cell Culture and Generation of Stable Cell Lines

NIH 3T3 cells were grown in Dulbecco's Modified Eagle's Medium (DMEM) with 10% bovine calf serum, penicillin, and streptomycin. Smo null (Smo−/−) mouse embryonic fibroblasts (MEFs) were grown in DMEM supplemented with 10% fetal bovine serum, penicillin, and streptomycin. To generate stable lines, mouse Smoothened (mSmo) constructs were subcloned into a vector for lentiviral production, bearing a C-terminal mCherry tag. Replication-defective lentiviruses were packaged in 293T cells, using standard protocols. Supernatants containing the virus were used to infect Smo−/− cells, followed by antibiotic selection beginning 48 hr post-infection (50 μg/mL blasticidin). After selection for 2 days, the cell cultures were expanded, and cells expressing low levels of mCherry-tagged mSmo were obtained by fluorescence-activated cell sorting.

METHOD DETAILS

Reagents

The following reagents were purchased: SAG (≥98%) from Axxora; SANT1 (≥95%) from Calbiochem; cyclopamine (> 99%) from LC Laboratories; BODIPY-cyclopamine from Toronto Research Chemicals; BODIPY-FL N-hydroxysuccinimide ester from Thermo Fisher; pravastatin (≥98%), cholesterol, cholesteryl hemisuccinate and methyl-β-cyclodextrin (MCD) from Sigma; cholestanol (98%) from Alfa Aesar; 20(S)-hydroxycholesterol (≥98%) and 25-fluorocholesterol (≥98%) from Steraloids; F7-Cholesterol (> 99%) from Avanti Polar Lipids. The oxysterol analogs, 20(S)-OHC-Pent and 20(R)-OHC-Pent (Nedelcu et al., 2013), were synthesized by Grignard reaction of pregnenolone with n-pentylmagnesium bromide. The product was purified by chromatography on silica gel (gradient elution, 0%–70% EtOAc/hexane), to provide a mixture of the R and S diasteromers. This mixture was subjected to normal phase chiral HPLC purification (6% *i*-PrOH/Hexane, on a RegisCell column), to yield the pure diastereomers. To prepare water-soluble sterol-MCD complexes (Gimpl et al., 1995), a sterol solution (40 mM in ethanol) was added, in portions, to a solution of MCD (40 mM in water). The mix was filter-sterilized, and the solvent was removed by evaporation under reduced pressure. The dried sterol-MCD complexes were then dissolved in sterile water, to a final concentration of 2.5 mM sterol. For cholesterol, cholestanol, 25-fluorocholesterol, cyclopamine, and 20(S)-hydroxycholesterol the molar ratio of MCD to sterol was 10:1, while for F7-cholesterol, due to its reduced solubility, the ratio was 25:1.

Antibodies

Rabbit anti-mCherry (Nedelcu et al., 2013) and anti-mSmo (Tukachinsky et al., 2010) antibodies were described before. The monoclonal mouse anti-acetylated tubulin antibody was purchased from Sigma.

Hh Pathway Assays

For qPCR assays, confluent cultures of NIH 3T3 cells or MEFs were starved overnight in DMEM, after which they were incubated for 24 hr in DMEM supplemented with the desired agents. Sterols were added as soluble MCD complexes, while more soluble compounds (oxysterols or SAG) were added from DMSO stocks. Cyclopamine was added from DMSO stock, except in the experiment testing activation of mSmoD477G/E522K, in which it was added as MCD complex. As Shh source, we used serum-free conditioned media from 293T cells transiently transfected with an expression construct encoding amino acids 1-197 of human Shh (Nedelcu et al., 2013). Ligand thus generated was added to cells diluted in fresh DMEM. Following incubation, cells were harvested and total RNA was isolated with RNA-Bee reagent (TelTest). After treatment with RNase-free DNase (Promega) and a second round of RNA-Bee purification, the RNA was reverse transcribed using Transcriptor reverse transcriptase and random hexamers (Roche). Transcription of mouse Gli1 gene was measured by qPCR, using FastStart SYBR Green Master reagent (Roche) on a Rotor-Gene 6000 (Corbett Robotics), as described (Nedelcu et al., 2013). Relative gene expression was calculated using a Two Standard Curve method in which the gene-of-interest was normalized to the *Ribosomal Protein L27* gene. The sequences for gene-specific primers are: *L27*: 5′-GTCGAGATGGGCAAGTTCAT-3′ and 5′-GCTTGGCGATCTTCTTCTTG-3′, *Gli1*: 5′-GGCCAATCACAAGTCAAGGT-3′ and 5′-TTCAGGAGGAGGGTACAACG −3′. All qPCR experiments were done in triplicate starting from three cell cultures, with error bars indicating SD.

Luciferase reporter assays were performed in Shh Light II cells (Taipale et al., 2000), as described (Tukachinsky et al., 2012). Confluent cell cultures were starved overnight in DMEM, after which they were incubated for 36 hr in DMEM supplemented with the desired compounds, followed by luciferase activity measurements. Each luciferase experiment was performed in quadruplicate starting from four biological replicates, and error bars represent the SD.

Sterol Depletion and Rescue Experiments

To deplete sterols, confluent cultures were first starved in DMEM overnight, after which they were incubated for 30 min with 1.5% MCD in DMEM. All subsequent incubations were done in DMEM supplemented with 40 μM pravastatin (to block sterol synthesis), with or without the indicated additives. For rescue experiments, sterols were delivered by incubating the cells for 1 hr with water-soluble MCD-sterol complexes (unless otherwise indicated, at a concentration of 100 μM in DMEM supplemented with 40 μM pravastatin). The cells were then incubated overnight with the desired agents, and were processed for immunofluorescence, qPCR or luciferase assay.

Immunofluorescence and Measurements of Smo Ciliary Localization

Cells were grown on glass coverslips and immunofluorescence was performed as described (Nedelcu et al., 2013). The primary antibodies used were: mouse anti-acetylated tubulin monoclonal antibody (cilia marker, 1:5000 dilution) and rabbit anti-mSmo polyclonal antibody (final concentration 1 μg/mL). Ciliary intensity of endogenous Smo was measured using custom automated image analysis software implemented in MATLAB (Nedelcu et al., 2013). Images used for automated analysis were acquired on a Nikon TE2000E microscope controlled by Metamorph software (Applied Precision), using a 40x PlanApo 0.95NA air objective (Nikon). Between 300 and 1000 cilia were analyzed per condition. Ciliary intensities are represented as boxplots, with the lower and upper bounds corresponding to the 25th and 75th quantiles respectively, and the horizontal line indicating the median intensity.

BODIPY-Cyclopamine Binding Assays

Binding of mSmo-mCherry fusions to BODIPY-cyclopamine was performed as described(Nedelcu et al., 2013). Briefly, mSmo constructs were expressed in 293T cells by transient transfection. The cells were washed with serum-free media (OptiMEM, Thermo Fisher) and were incubated for 1 hr in OptiMEM supplemented with 20 nM BODIPY-cyclopamine, in the presence or absence of competitor drug. The cells were fixed in PBS with 3.6% formaldehyde for 30 min at room temperature, followed by several washes with TBST (10 mM Tris [pH 7.5], 150 mM NaCl, 0.2% Triton X-100). The cells were then imaged by epifluorescence microscopy.

Sterol Affinity Matrices

Preparation of Affigel-10 coupled to 20(S)-hydroxycholesterol and Affigel-10 control beads was described before (Nedelcu et al., 2013). Similar method was used to prepare other sterol affinity matrices. Affigel-10 beads (BioRad) were converted to primary amine beads, by reaction with 4,7,10-trioxa-1,13-tridecanediamine (0.5 M in dry isopropanol), for 3 hr at room temperature. The amine beads were washed extensively with isopropanol, to remove excess unreacted diamine, and were resuspended in dry isopropanol. N-hydroxysuccinimide (NHS) esters of either C19-position carboxylic acid derivative of cholesterol, or of cholesteryl hemisuccinate, were dissolved in dry DMSO and were added to the beads (20 mM final concentration), followed by addition of dry triethylamine (100 mM). The beads were incubated overnight at room temperature, with tumbling. The beads were washed with DMSO and isopropanol, to remove unreacted NHS esters. Before use, the beads were washed with distilled water, and then with lysis buffer (20 mM HEPES [pH 7.5], 150 mM NaCl, 0.5% dodecyl-β-maltoside).

Sterol Affinity Assays

Sterol affinity assays were performed using either mSmo-mCherry fusions expressed in 293T cells (Nedelcu et al., 2013), or XSmo ectodomain expressed and purified from bacteria. Briefly, mSmo-mCherry fusions were expressed in 293T cells, either stably or by transient transfection. The cells were lysed for 30 min on ice in lysis buffer supplemented with protease inhibitors (Roche), and the detergent extract was clarified by centrifugation at 21,000 g. The extract was then incubated for 30 min at room temperature with the desired competitor compound dissolved in DMSO, or just DMSO control. Sterol beads or control beads were added to extracts, and the mix was incubated for 1 hr at 4°C, with tumbling. The beads were pelleted and were washed 3 times with wash buffer (20 mM HEPES [pH 7.5], 150 mM NaCl, 0.2% dodecyl-β-maltoside). Bound material was eluted in sample buffer with DTT, separated by SDS-PAGE and subjected to immunoblotting with anti-mCherry antibodies. Some sterol affinity assays employed XSmo ectodomain (amino acids 35-189) expressed and purified from bacteria (see below). XSmo ectodomain was incubated with competitor compounds in binding buffer (20 mM Tris-HCl [pH 7.5], 150 mM NaCl, 0.2% Triton X-100) for 30 min at room temperature, followed by addition of beads and incubation at room temperature for 1 hr, with tumbling. The beads were washed 3 times with binding buffer, and bound protein was analyzed by SDS-PAGE followed by Coomassie staining.

Recombinant Protein Expression and Purification

Fragments of *Xenopus laevis* Smoothened (XSmo) comprising only the cysteine-rich domain (CRD, residues 35-154) or the ectodomain (residues 35-189) were subcloned into pET-32a bacterial expression vector (Millipore). The final constructs contained an N-terminal thioredoxin-His_6-S-tag, followed by enterokinase and TEV protease cleavage sites, followed by the XSmo sequence. The fusions were expressed as soluble proteins in Rosetta-gami 2 *E. coli* cells (Millipore), by overnight induction with 0.1 mM IPTG, at 16°C. Induced bacterial cells were harvested and lysed in 20 mM Tris-HCl (pH 8.0), 500 mM NaCl, 20 mM imidazole,

10% glycerol and 0.1% Triton X-100. The clarified supernatant was loaded on a 5 mL Ni-NTA agarose column (QIAGEN) pre-equilibrated with lysis buffer, followed by washing with 20 column volumes of lysis buffer. Triton X-100 was then removed by washing with 5 column volumes of buffer containing 20 mM Tris-HCl (pH 8.0), 500mM NaCl, 50mM imidazole, 10% glycerol and 0.5% n-octyl-β-D-glucoside. The protein was then eluted in 30 mL elution buffer, consisting of 20 mM Tris-HCl (pH 8.0), 500 mM NaCl, 250 mM imidazole, 10% glycerol and 0.5% n-octyl-β-D-glucoside. The eluate was diluted into 200 mL of redox buffer containing 20 mM Tris-HCl (pH 8.5), 200 mM NaCl, 5% glycerol, 10 mM EDTA, 0.05% n-octyl-β-D-glucoside, 5 mM reduced glutathione and 0.5 mM oxidized glutathione. After stirring at room temperature for 12 hr to promote disulfide bond formation, the protein was concentrated and fractionated by size exclusion chromatography on a HiLoadTM 16/60 SuperdexTM 200 prep grade column (GE Healthcare). The peak corresponding to monomeric protein was collected, and was digested overnight with TEV protease. The cleaved thioredoxin fusion tag was removed by passage through a Ni-NTA column, and untagged XSmoCRD was further purified by size exclusion chromatography in a buffer containing 20 mM HEPES (pH 7.5) and 100 mM NaCl.

Crystallization, Data Collection, and Structure Determination

Purified XSmoCRD, with or without added 20(S)-OHC or cyclopamine (20 μM), was concentrated to 10-15 mg/mL in 20 mM HEPES (pH 7.5) and 100 mM NaCl. Crystals were grown in hanging drops at 22°C, by mixing protein samples 1:1 with reservoir solution. Apo XSmoCRD crystals were grown in 0.2 M zinc acetate and 20% PEG 3350. Co-crystals of XSmoCRD with 20(S)-OHC were grown in 0.15 M potassium bromide and 30% PEG MME 2000. XSmoCRD-cyclopamine co-crystals were grown in 0.1M HEPES (pH 7.5) and 25% PEG 3350. Crystals were harvested and flash frozen in liquid nitrogen, using crystallization reservoir buffer supplemented with 20% glycerol as cryoprotective solution. X-ray diffraction data were collected using the APS beamline SBC-CAT 19-ID at the Argonne National Laboratory, and were processed with HKL-3000 (Minor et al., 2006). All structures were solved by molecular replacement in the program PHASER (McCoy et al., 2007). ZfSmoCRD structure (PDB ID: 4C79) was used as search model to find the solution for the structure of XSmoCRD bound to 20(S)-OHC. The initial model was built automatically using the program AutoBuild in PHENIX and the ligand was located by LigandFit. The complex model thus generated was manually rebuilt in COOT (Emsley and Cowtan, 2004) and refined using PHENIX. This structure, with 20(S)-OHC removed, subsequently served as search model to determine the structures of apo XSmoCRD and XSmoCRD-cyclopamine, following similar procedures, except that the CCP4 program ARP/wARP was used to build the automatic model for apo XSmoCRD structure. All structure figures were prepared in PyMol. Data collection and refinement statistics are summarized in Table S1.

Fluorescence Polarization-Based Ligand Binding Assays

BODIPY FL-labeled 20(S)-OHC, cyclopamine or 22-azacholesterol (5nM) were added to purified XSmoCRD or XSmo ectodomain, in buffer containing 20 mM HEPES (pH 7.5) and 100 mM NaCl, and were incubated for 1 hr at room temperature. For competition experiments, purified XSmo ectodomain (1.5 μM) was incubated with BODIPY-cyclopamine (5 nM), in the presence or absence of varying concentrations of unlabeled compounds, for 1 hr at room temperature. Fluorescence polarization was then measured using a SpectraMax M5 microplate reader, and was converted to anisotropy values. All measurements were performed in triplicate, and Kd and IC_{50} values were calculated by fitting the binding curves in GraphPad Prism 5. For figure preparation, anisotropy data were normalized and plotted as fraction bound values.

Circular Dichroism Temperature Melting Experiments

Purified XSmo ectodomain was incubated overnight in the presence of the indicated small molecules (25 μM final concentration, added from 10 mM stocks in DMSO). The protein samples were then purified by size exclusion using a G-25 column. The final protein concentration was adjusted to 0.2 mg/mL, in a buffer consisting of 10 mM Na phosphate (pH = 7.5) and 100 mM NaCl. Circular dichroism (CD) melting experiments were carried out on a Jasco J-815 CD spectrometer using a 1 mm cuvette. The CD signal at 225 nm was continuously recorded in 1°C increments between 25°C and 95°C, with 1°C/min ramp rate and 1 min equilibration time. To calculate melting temperatures (T_m), the data points were converted to the corresponding denatured fractions and were fitted in KaleidaGraph, as described(Greenfield, 2006).

Chemical Synthesis

General Methods for Chemical Synthesis

All solvents and reagents were obtained from commercial sources and were used as such. NMR spectra were recorded on a Varian Oxford 600 MHz NMR spectrometer. NMR chemical shifts are expressed in ppm relative to internal solvent peaks, and coupling constants are measured in Hz. LC/MS was performed on a Waters Micromass ZQ instrument using an ESI source coupled to a Waters 2525 HPLC system operating in reverse mode with a Waters SunfireTM C185 uM 4.6 × 50 mm column. Flash chromatography was performed on silica gel columns using a Biotage Isolera One flash purification system.

Synthesis of BODIPY-22-azacholesterol

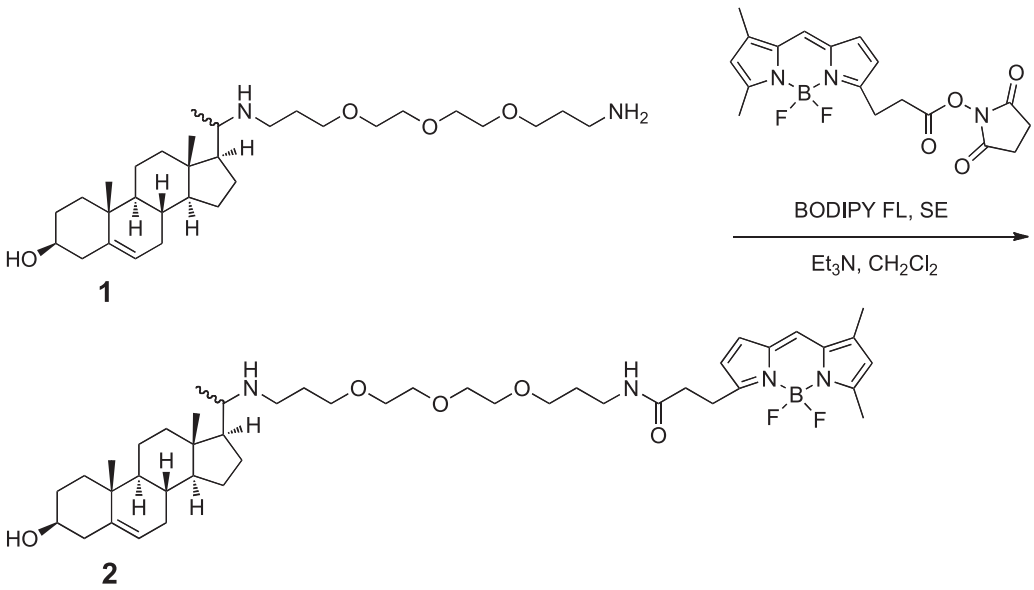

Triethylamine (3.6 μL, 51.4 μmol) and BODIPY-FL N-hydroxysuccinimide ester (10.0 mg, 25.7 μmol) were added to a solution of amine **1** (Nedelcu et al., 2013) (16.1 mg, 30.8 μmol) in dichloromethane (800 μL). The reaction mixture was stirred at room temperature for 12 hr and then evaporated to dryness under a stream of nitrogen gas. Purification by flash chromatography (SiO_2, stepwise gradient from 100:1 to 85:15 CH_2Cl_2/MeOH) yielded the desired product **2** as a dark red solid (19.8 mg, 96.9%).

Compound 2: ^{1}H NMR (600 MHz, $CDCl_3$): δ 7.08 (s, 1H), 6.87 (d, *J* = 4.0 Hz, 1H), 6.53-6.49, 6.40-6.35 (1:1.8; m, 1H), 6.31-6.27 (m, 1H), 6.10 (s, 1H), 5.33-5.30 (m, 1H), 3.63-3.51 (m, 9H), 3.51-3.46 (m, 3H), 3.33-3.28 (m, 2H), 3.26 (t, *J* = 7.2 Hz, 2H), 3.18-2.97 (m, 2H), 2.94-2.83 (m, 1H), 2.74-2.67 (m, 1H), 2.62-2.57 (m, 2H), 2.54 (s, 3H), 2.30-2.17 (m, 5H), 2.02-1.76 (m, 7H), 1.74-1.69 (m, 2H), 1.69-1.40 (m, 7H), 1.40-1.20 (m, 4H), 1.20-1.00 (m, 5H), 1.00-0.78 (m, 5H), 0.70, 0.67 (2.5:1; s, 3H); ^{13}C NMR (150 MHz, $CDCl_3$) (as the major diasteromer): δ 171.8, 160.1, 158.1, 143.9, 141.0, 135.2, 133.6, 128.6, 124.0, 121.6, 120.5, 117.6, 71.8, 70.7, 70.7, 70.5, 70.5, 70.4, 70.3, 70.3, 69.9, 69.8, 56.3, 55.8, 50.0, 44.3, 42.4, 42.2, 37.8, 37.4, 36.7, 36.0, 31.9, 31.9, 31.8, 29.3, 25.0, 24.2, 21.2, 19.6, 19.6, 15.1, 12.5, 12.2, 11.5; LC/MS: (ESI, m/z) calculated $[M+H]^+$ for $C_{45}H_{69}BF_2N_4O_5$: 795.5, found 795.67.

Synthesis of BODIPY-20(S)-hydroxycholesterol

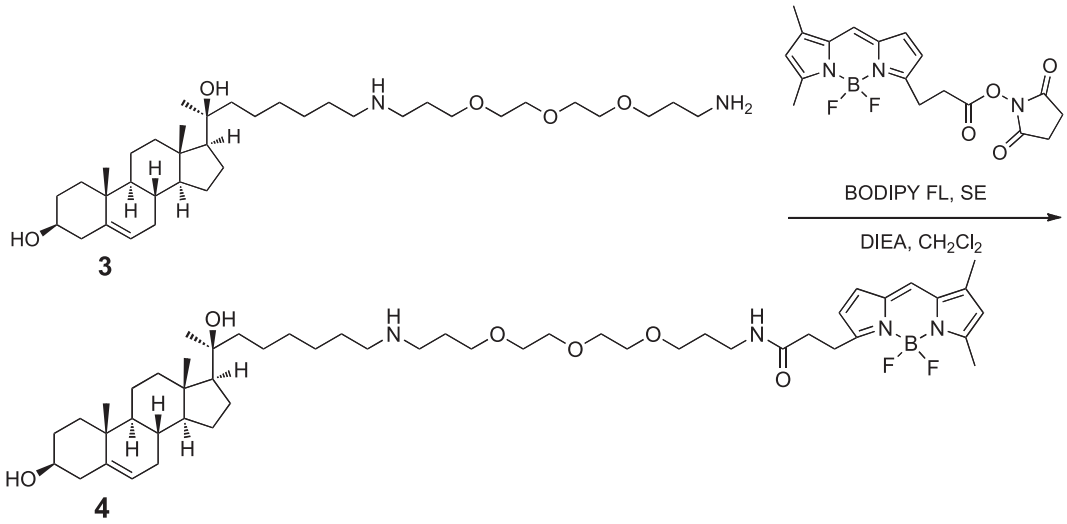

Diisopropylethylamine (11.2 μL, 64.2 μmol) and BODIPY FL *N*-hydroxysuccinimide ester (5.0 mg, 12.8 μmol) were added to a solution of amine **3** (Nedelcu et al., 2013) (13.1 mg, 15.4 μmol) in dichloromethane (600 μL). The reaction mixture was

stirred at room temperature for 2 hr and then evaporated to dryness under a stream of nitrogen gas. Purification by flash chromatography (SiO_2, stepwise gradient from 100:1 to 85:15 CH_2Cl_2/MeOH) yielded the desired amide **4** as a dark red solid (9 mg, 47%).

Compound 4: ^{1}H NMR (600 MHz, $CDCl_3$): δ 7.09 (s, 1H), 6.88 (d, *J* = 4.2 Hz, 1H), 6.62-6.57 (m, 1H,), 6.31 (d, *J* = 4.2 Hz, 1H), 6.10 (s, 1H), 5.35-5.33 (m, 1H), 3.62-3.53 (m, 8H), 3.53-3.47 (m, 2H), 3.33-3.29 (m, 2H), 3.26 (t, *J* = 7.8 Hz, 2H), 3.07-3.03 (m, 2H), 2.90-2.85 (m, 2H), 2.62 (t, *J* = 7.8 Hz, 2H), 2.60-2.53 (m, 3H), 2.30-2.18 (m, 5H), 2.08-2.05 (m, 1H), 2.01-1.93 (m, 3H), 1.85-1.80 (m, 2H), 1.75-1.66 (m, 4H), 1.65-1.55 (m, 3H), 1.55-1.44 (m, 5H), 1.44-1.36 (m, 3H), 1.35-1.15 (m, 6H), 1.15-1.05 (m, 5H), 1.01-0.95 (m, 4H), 0.94-0.78 (m, 9H), 0.78-0.69 (m, 2H); ^{13}C NMR (150 MHz, $CDCl_3$) (as the major diasteromer): δ172.0, 160.0, 158.1, 143.8, 140.9, 135.1, 133.5, 128.5, 123.9, 121.7, 120.4, 117.6, 75.2, 71.9, 70.6, 70.2, 70.1, 70.1, 69.6, 69.6, 58.0, 57.0, 50.2, 47.8, 46.7, 43.8, 42.4, 40.3, 37.5, 37.4, 36.6, 35.8, 32.1, 31.9, 31.8, 31.5, 29.8, 29.3, 26.9, 26.4, 25.9, 25.0, 24.1, 23.9, 22.8, 22.5, 21.1, 19.5, 15.1, 13.7, 11.5; LC/MS: (ESI, m/z) calculated $[M+H]^+$ for $C_{51}H_{81}BF_2N_4O_6$: 895.6, found 896.

Synthesis of Cholesterol Analog with Handle Attached to C19

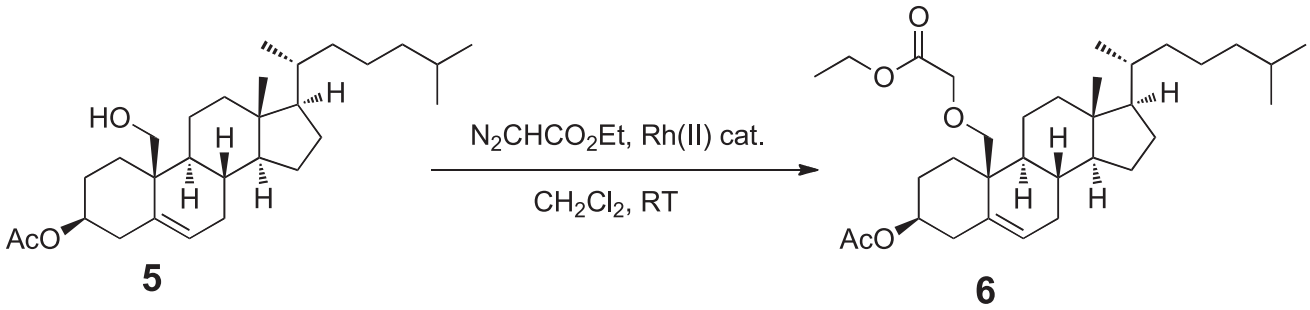

Compound **5** (19-hydroxycholesteryl acetate) was prepared as described (Jao et al., 2015). To a stirred solution of compound 5 (2 g, 4.5 mmol) in dry dichloromethane (50 mL) was added $Rh(II)(OAc)_2$ (20 mg, 0.01 equivalents). Ethyl diazoacetate (0.6 mL, 1.05 equivalents) was then added drop-wise over one hour. The reaction mix was stirred overnight at room temperature, under nitrogen. The solvent was evaporated under reduced pressure, and the product (TLC: 20% ethyl acetate/hexane, R_f = 0.38, 2% H_2SO_4/EtOH stain) was purified by flash chromatography (5%–40% linear gradient ethyl acetate/hexane). Compound **6** (3β-acetyl, 19-cholesteryl ethyl acetate ether) was obtained as clear oil, which formed clear needles upon standing (1.65 g, 69%).

1H NMR (600 MHz, CDCl3): δ 5.58 (1H, d, 6-H, vinylic), 4.60 (1H, m, 3α-H), 4.17 (2H, q), 4.02 (2H, s), 3.73 (1H, d), 3.46 (1H, d), 2.36 (2H, m), 2.08 (1H, m), 1.98 (3H, s), 1.25 (3H, t), 0.69 (3H, s); 13C NMR (600 MHz, CDCl3): δ 170.52, 170.43, 135.61, 126.25, 73.70, 72.77, 68.85, 60.68, 57.36, 56.18, 50.39, 42.52, 40.80, 40.10, 39.58, 38.42, 36.26, 35.86, 33.34, 32.86, 31.63, 28.29, 28.08, 28.05, 24.24, 23.89, 22.87, 22.61, 21.77, 21.41, 18.75, 14.28, 11.99.

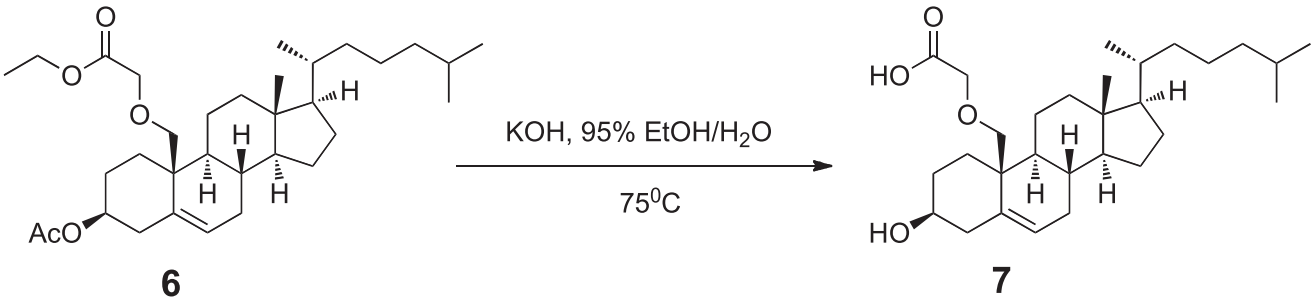

Compound **6** (220 mg, 0.41 mmol) was added to a solution of KOH (1.12 g) in 95% ethanol (20 mL). The mix was stirred at 85°C for 2 hr, after which it was chilled on ice and was neutralized with hydrochloric acid. The crude product was extracted twice with dichloromethane, the organic layers were combined, dried over Na_2SO_4, filtered, and the solvent was evaporated under reduced pressure. The product (TLC: 10% MeOH/$CHCl_3$ + 0.5% AcOH, R_f = 0.17, 2% H_2SO_4/EtOH) was purified by flash chromatography (2% MeOH/$CHCl_3$ + 0.5% AcOH), to yield compound **7** (19-cholesteryl acetic acid ether) as a white solid (123 mg, 65%). A second, larger scale reaction started with 1.65 g (3.1 mmol) compound **6** and yielded 1.3 g compound **7** (91%).

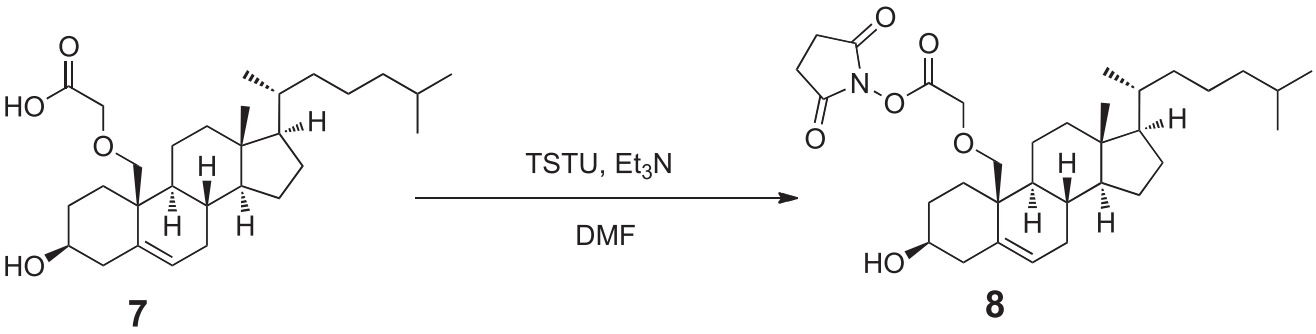

7 8

Compound **7** (123 mg, 0.27 mmol) was dissolved in dry DMF (3 mL), followed by addition of TSTU (101.3 mg) and triethylamine (0.74 mL). The reaction was stirred overnight under nitrogen, after which the solvent was evaporated under reduced pressure. The product (TLC: 80% ethyl acetate/hexane, R_f = 0.32, 2% H_2SO_4/EtOH) was purified by flash chromatography (linear gradient 40%–80% ethyl acetate/hexane), to yield **8** (19-cholesteryl N-hydroxysuccinimide acetic acid ether) as white crystals (33 mg, 22%). A second, scaled-up reaction started with 1.27 g (2.76 mmol) compound **7** and resulted in 755 mg compound **8** (49%).

1H NMR (400 MHz, CDCl3): δ 5.59 (1H, d, 6-H, vinylic), 4.41 (2H, s), 3.80 (1H, d), 3.59 (3H, m), 3.10 (2H, s), 3.00 (2H, s), 0.69 (3H, s). 13C NMR (400 MHz, CDCl3): δ 168.93, 166.04, 147.38, 134.23, 125.68, 102.68, 76.84, 73.33, 71.65, 66.78, 57.52, 56.30, 50.43, 42.61, 40.85, 40.20, 39.68, 36.35, 35.95, 33.54, 33.02, 32.02, 31.70, 28.39, 28.17, 25.75, 25.64, 24.32, 23.99, 22.97, 22.71, 21.99, 19.69, 18.85, 12.10.

QUANTIFICATION AND STATISTICAL ANALYSIS

Statistical parameters are reported in Figure Legends and in Method Details. Q-PCR experiments were done in triplicate starting from three cell cultures, with error bars indicating SD. Luciferase experiments were performed in quadruplicate starting from four biological replicates, and error bars represent the SD. For measuring Smo localization to cilia, at least 300 cilia were analyzed for each treatment. Smo intensity at cilia is displayed as boxplots; the lower and upper bounds of the box represent the 25th and 75th percentile of intensity distribution, and the horizontal line represents the median intensity. In graphs showing fraction of Smo-positive cilia, error bars represent the sub-sampling SD of the fraction of positive cilia; this is calculated by dividing the cilia analyzed for each condition into five random non-overlapping sub-samples, calculating the fraction of positive cilia in each sub-sample, and then calculating SD of the fraction of positive cilia across sub-samples.

DATA AND SOFTWARE AVAILABILITY

Data Resources

Accession numbers for the atomic coordinates for apo XSmoCRD, XSmoCRD-20(S)-OHC, and XSmoCRD-cyclopamine structures reported in this paper are PDB: 5KZZ, 5KZV, and 5KZY, respectively.

Cell

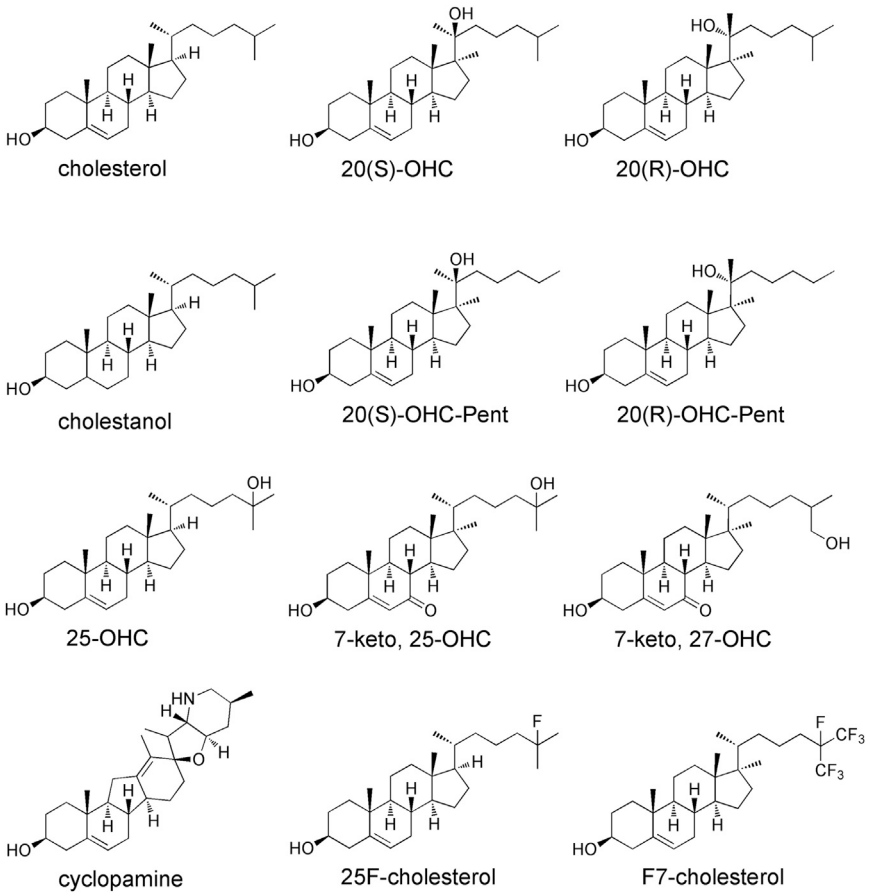

Figure S1. SmoCRD Ligands, Related to Figures 1–6

Shown are chemical structures of sterols, oxysterols, cyclopamine, and fluorinated sterols used in this study.

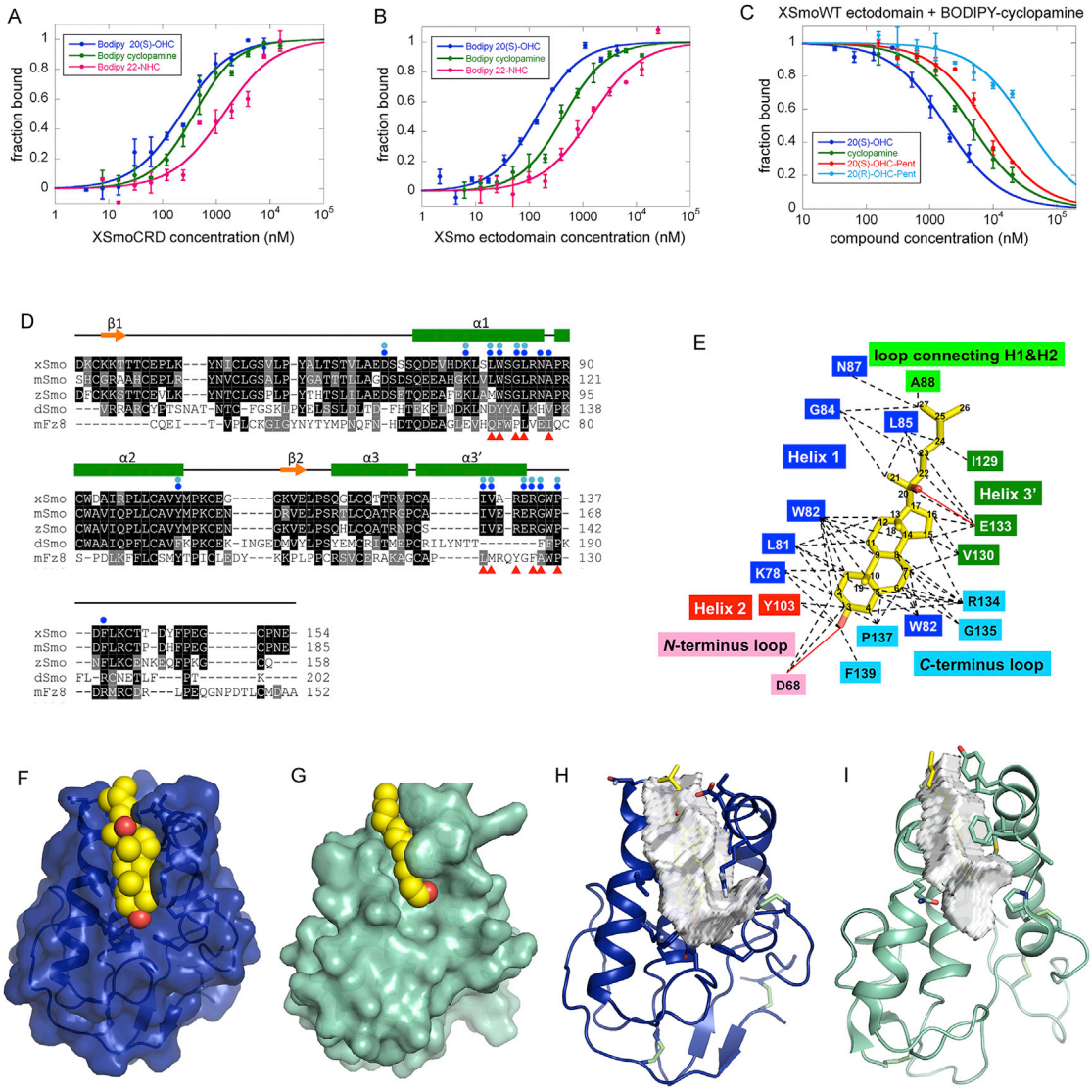

Figure S2. Sterol Recognition by XSmoCRD and Comparison with Palmitate Recognition by mFz8CRD, Related to Figure 1

(A–C) Sterol binding to XSmoCRD and XSmo ectodomain measured by fluorescence polarization (FP). Purified XSmoCRD (amino acids 35-154) or ectodomain (amino acids 35-189) were mixed with small molecule-BODIPY probes, followed by FP measurement. (A) Increased amounts of XSmoCRD were incubated with the indicated BODIPY probes. XSmoCRD binds BODIPY-20(S)-OHC (Kd = 225 nM), BODIPY-cyclopamine (Kd = 389 nM), and BODIPY-22-NHC (Kd = 1.36 μM). (B) As in (A), but with XSmo ectodomain. XSmo ectodomain binds BODIPY-20(S)-OHC (Kd = 138 nM), BODIPY-cyclopamine (Kd = 434 nM), and BODIPY-22-NHC (Kd = 1.4 μM). XSmoCRD and XSmo ectodomain have very similar sterol-binding properties. (C) XSmo ectodomain was incubated with BODIPY-cyclopamine in the presence of the indicated concentrations of competitors. XSmo ectodomain binding to BODIPY-cyclopamine is competed by 20(S)-OHC (IC_{50} = 1.8 μM) and cyclopamine (IC_{50} = 4.5 μM), and is competed by 20(S)-OHC-Pent diastereomer (IC_{50} = 8 μM) preferentially over 20(R)-OHC-Pent diastereomer (IC_{50} = 34 μM).

(D and E) Amino acid contacts involved in recognition of sterols by Smo. (D) Structural alignment of XSmo CRD (this study), mSmoCRD, zfSmoCRD (PDB ID 4C79), *Drosophila* SmoCRD (PDB ID 2MAH), and mFz8CRD (PDB ID 4F0A). Blue circles indicate XSmo residues that interact with 20(S)-OHC, while cyan circles indicate interactions with cyclopamine. Red triangles indicate mFz8CRD residues that contact the palmitoyl moiety of XWnt8(Janda et al., 2012). Secondary structure of XSmoCRD is shown above the alignment. The sequences were aligned using SALIGN (Braberg et al., 2012). (E) XSmo amino acids that contact 20(S)-OHC. Residues are color coded to indicate the secondary structure element in XSmoCRD that they belong to.

(F–I) Comparison between structure of XSmoCRD-20(S)-OHC and mFz8CRD-palmitate. (F) Surface representation of XSmoCRD bound to 20(S)-OHC (shown as space-filling model). (G) Surface representation of mFz8CRD bound to the palmitoyl moiety of XWnt8. (H) The total volume of the sterol-binding site in XSmoCRD is 604Å^3, compared to a volume of 527 Å^3 for 20(S)-OHC. The total buried surface area for the XSmoCRD-20(S)-OHC interaction is 788 Å^2 (454 Å^2 from the ligand and 334 Å^2 from the CRD). The exposed hydrophobic regions of the ligand (172 Å^2, including the β face and distal portion of the isooctyl tail) may interact with other parts of full-length XSmo, to provide additional shielding from aqueous environment. Volumes were calculated using the 3V program (Voss and Gerstein, 2010). (I) The total volume of the binding site in mFz8CRD is 375Å^3, compared to a volume of 331 Å^3 for palmitate. The small volume of the ligand-binding site in mFz8 makes it incompatible with sterol binding.

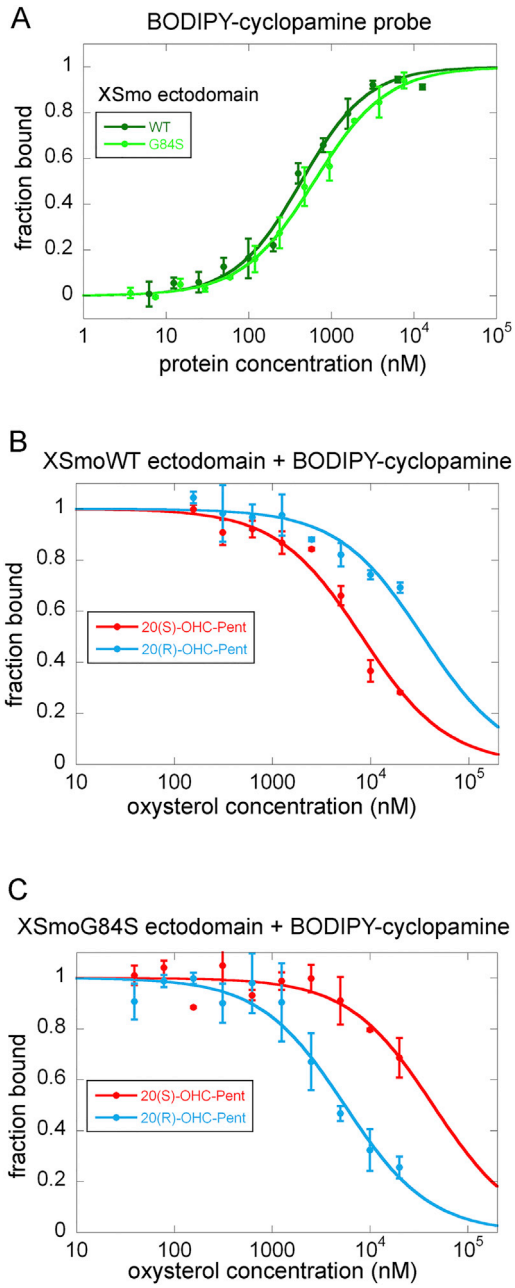

Figure S3. Reversing Oxysterol Diastereospecificity of XSmo, Related to Figure 2

(A) Increased amounts of purified XSmo or XSmoG84S ectodomain were incubated with BODIPY-cyclopamine, and the FP signal was measured. XSmo and XSmoG84S ectodomain bind BODIPY-cyclopamine with comparable affinity (Kd = 434 nM and Kd = 621 nM).

(B) Purified XSmo ectodomain was incubated with BODIPY-cyclopamine in the presence of the indicated concentrations of competitors. XSmo ectodomain binding to BODIPY-cyclopamine is competed by 20(S)-OHC-Pent (IC_{50} = 8 μM) preferentially over 20(R)-OHC-Pent (IC_{50} = 34 μM).

(C) As in (B), but with XSmoG84S ectodomain. XSmoG84S ectodomain binding to BODIPY-cyclopamine is competed by 20(R)-OHC-Pent (IC_{50} = 5.5 μM) preferentially over 20(S)-OHC-Pent (IC_{50} = 44 μM).

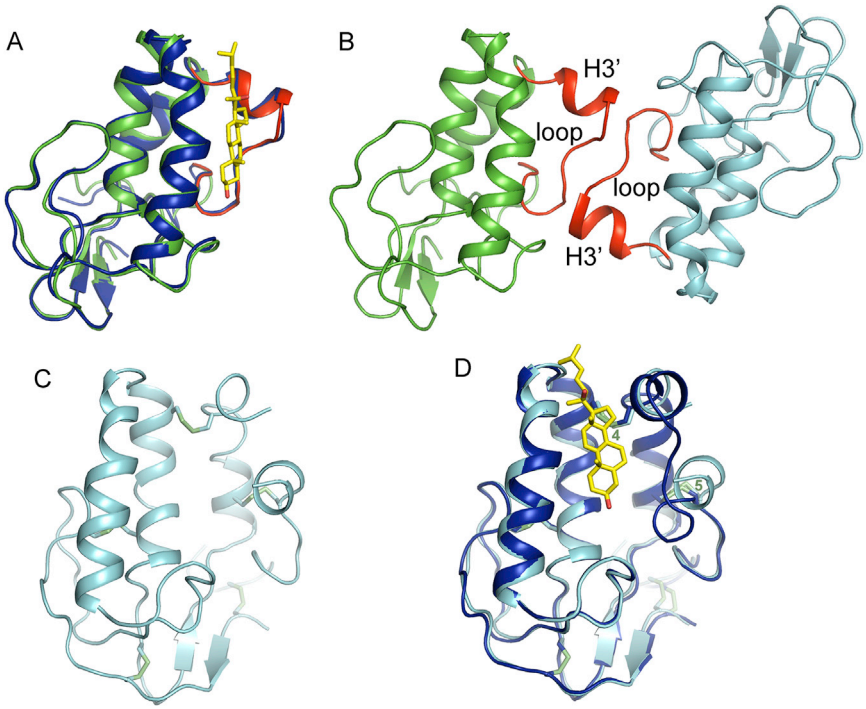

Figure S4. Sterol-Induced Conformational Change in XSmoCRD, Related to Figure 3

(A) Comparison between XSmoCRD-20(S)-OHC and apo zfSmoCRD structures. Unliganded zfSmoCRD (green) (PDB ID 4C79) superimposed on XSmoCRD (navy) bound to 20(S)-OHC (yellow), showing that the two proteins adopt very similar conformations.

(B) Crystal packing of unliganded zfSmoCRD (PDB ID 4C79). Helix 3′ and the subsequent loop (red), which together constitute half of the sterol-binding groove, are involved in contacts with the same portion of the neighboring protein molecule, forming a 2-fold symmetric dimer. This suggests that the ligand-binding site in apo zfSmoCRD might artifactually adopt a "closed" conformation, mimicking the ligand-bound state.

(C) Ribbon diagram showing the overall structure of unliganded XSmoCRD.

(D) Superimposition of unliganded XSmoCRD (cyan) and 20(S)-OHC-bound XSmoCRD (navy). The protein undergoes a dramatic conformational change upon oxysterol (yellow) binding, involving the polypeptide stretch between disulfide bonds 4 and 5.

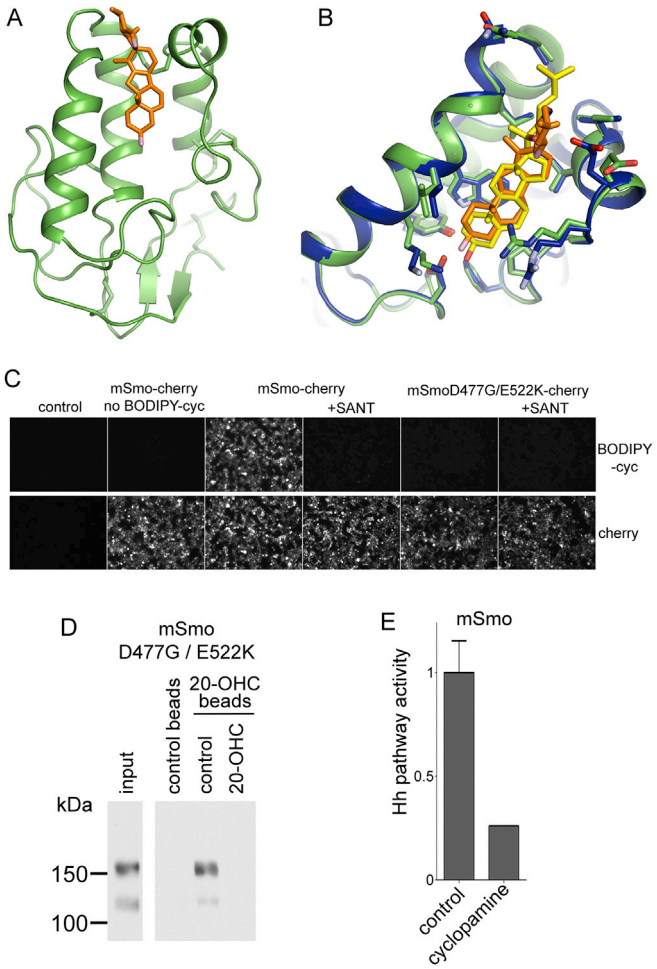

Figure S5. Cyclopamine-Induced Conformational Change in XSmoCRD, Related to Figure 4

(A) Overall structure of XSmoCRD (green) in complex with the plant alkaloid, cyclopamine (orange).

(B) Close up view of cyclopamine (orange) bound to XSmoCRD (green), superimposed on 20(S)-OHC (yellow) bound to XSmoCRD (navy). Cyclopamine and 20(S)-OHC induce very similar conformations of the sterol-binding site.

(C) The mSmoD477G/E522K mutant does not bind BODIPY-cyclopamine. Cultured 293T cells expressing mCherry-tagged mSmo wild-type or mSmoD477G/E522K were incubated with BODIPY-cyclopamine (50 nM), in the presence or absence of SANT1 competitor (10 μM). The cells were fixed, washed, and BODIPY-cyclopamine and mCherry fusions were imaged by fluorescence microscopy. The mSmoD477G/E522K mutant does not bind BODIPY-cyclopamine, in contrast to wild-type mSmo.

(D) The mSmoD477G/E522K mutant still binds oxysterols. MCherry-tagged mSmoD477G/E522K was expressed in 293T cells, and was assayed for binding to 20(S)-OHC affinity matrix (Nedelcu et al., 2013), in the absence or presence of free 20(S)-OHC competitor (100 μM). The mutant protein binds 20(S)-OHC beads and is competed by free 20(S)-OHC, but does not bind control beads (see Figure S6C for schematic of the beads used in this assay).

(E) Smo null MEFs rescued by stable expression of mCherry-tagged mSmo were incubated overnight in the absence of presence of cyclopamine (10 μM), and Hh pathway activity was assayed by qPCR for endogenous Gli1 mRNA. Error bars indicate SD (n = 3). As expected, cyclopamine inhibits wild-type mSmo.

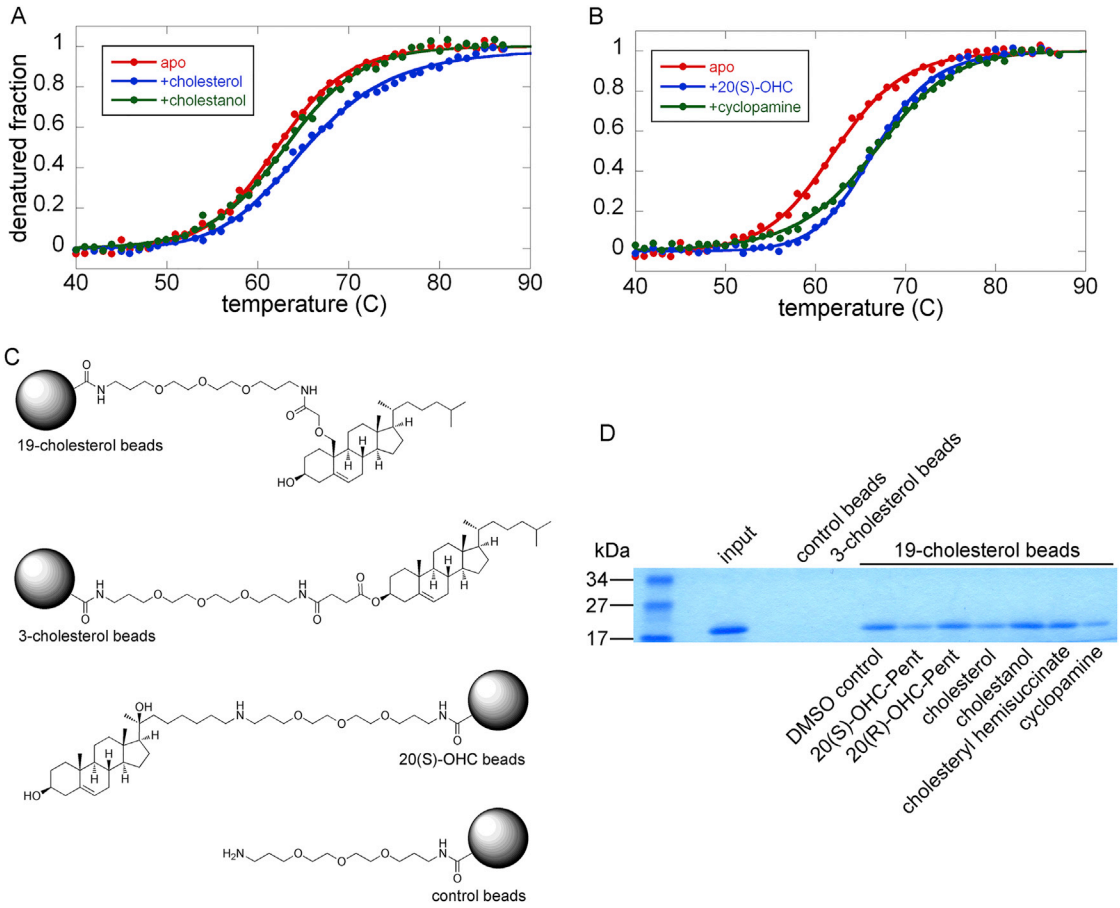

Figure S6. Smo Binds Cholesterol, Related to Figure 5

(A and B) Binding of XSmo ectodomain to sterols measured by circular dichroism (CD) melting. Purified XSmo ectodomain was incubated in the absence or presence of the indicated small molecules, and thermal denaturation of the protein was measured by recording the CD signal at 225 nm as a function of temperature. (A) The melting temperature of XSmo ectodomain (Tm = 62.1°C) is increased by cholesterol (Tm = 65.3°C), but not by cholestanol (Tm = 62.9°C), indicative of cholesterol binding. (B) XSmo ectodomain melting temperature is increased by binding to 20(S)-OHC (Tm = 66.5°C) or cyclopamine (Tm = 66.6°C).

(C) Schematic of affinity resins used in this study. Sterol molecules are attached to Affigel beads via a linker with three ethylene glycol units. Attachment is through C-19 for 19-cholesterol beads, through the 3β-OH group for 3-cholesterol beads, and through the sterol tail for 20(S)-OHC beads. Beads derivatized with the ethylene glycol linker alone serve as negative control.

(D) XSmo ectodomain binds to 19-cholesterol affinity resin. Purified XSmo ectodomain was incubated with 19-cholesterol beads, in the presence of the indicated compounds (500 μM, added from 20 mM DMSO stocks). The beads were washed, and bound protein was eluted and analyzed by SDS-PAGE and Coomassie staining. Beads without attached sterols served as negative control. XSmo ectodomain does not bind 3-cholesterol beads, consistent with the requirement of a free 3β-OH group for XSmo binding (Nedelcu et al., 2013).

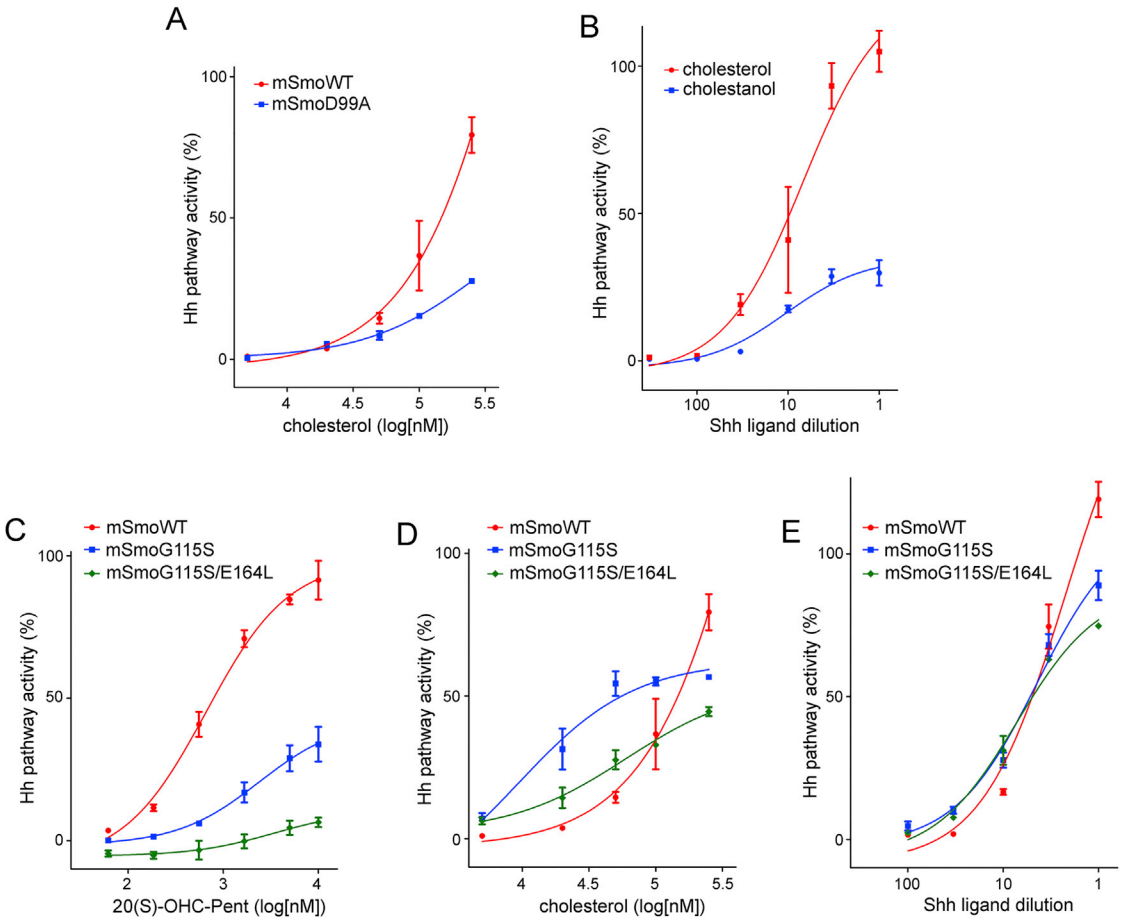

Figure S7. Cholesterol as Endogenous Activator of Smo, Related to Figure 6

(A) Hh pathway activation by cholesterol is defective in Smo null cells rescued with mSmoD99A, in contrast to cells rescued with wild-type mSmo. Hh signaling was assayed by qPCR for endogenous Gli1. Error bars indicate SD (n = 3). This experiment was performed in parallel with the ones in Figure 5B and Figure 6B, and shows the same curve for stimulation of wild-type mSmo by cholesterol.

(B) Shh synergizes with cholesterol, but not with cholestanol, to activate Hh signaling in Smo null cells rescued with wild-type mSmo. Sterols were added to 5 μM, as soluble MCD complexes.

(C–E) Responsiveness to 20(S)-OHC-Pent is reduced in Smo null cells rescued with mSmoG115S, compared to wild-type mSmo. Cells rescued with mSmoG115S/E164L do not respond to 20(S)-OHC-Pent. In contrast, cholesterol (D) and Shh (E) activate wild-type mSmo, mSmoG115S and mSmoG115S/E164L to a similar extent. Experiments in (C–E) were performed in parallel with experiments shown in Figures 6A–6C, thus the curves for wild-type mSmo are the same.